Ultrafast Optical Nonlinearity of Liquid Phase Exfoliated$Pdse_2$ Nanosheets

Manal Alotaibi

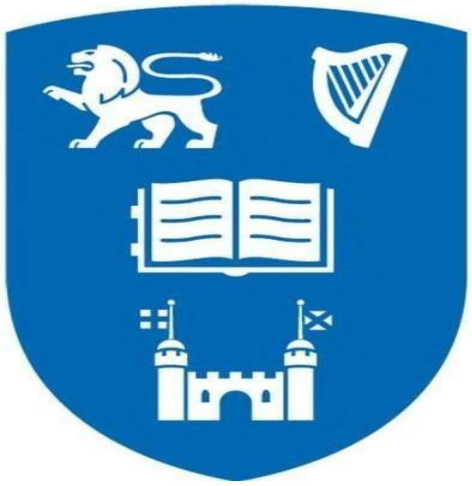

School of Physics and the Centre for Research on Adaptive Nanostructure and Nanodevices

(CRANN)

Supervised by

Prof. Werner Blau.

Trinity College Dublin

2022

Acknowledgments

I would like to thank every member of the Trinity School of Physics. In particular, I would like to thank, Prof. Johnathan Coleman, Prof. Hangzhou Zhang, Louise Bradley, Prof. David McCloskey, Jing Jing, Chris Smith, Kenneth Concannon, Helen O Halloran, and Una Dowling. A special thanks to Dr Colm Stephens for all his kindness to me.

It is hard to find the words to express my gratitude to my supervisor, Werner Blau, who has been very supportive and has helped me in so many ways. I would like to thank him for all the guidance he has given me, which allowed me to successfully complete my research.

Also, I would like to thank my friend Gaozhong Wang who has been so supportive during my two years of research, as well as to express my appreciation to Beata M. Szydłowska for preparing a sample for the University of Heidelberg.

Next, I would like to thank the Government of the Kingdom of Saudi Arabia for their support, which allowed me to study and research in Ireland. The scholarship granted to me was truly life changing. Also, I would like to thank Shaqra University for their continued support and understanding.

Finally, I would like to thank my family, who have been truly supportive. A special thanks to my daughters and my husband Khalid.

Declaration

I declare that this thesis has not been submitted as an exercise for a degree at this or any other university and it is entirely my own work. I agree to deposit this thesis in the University's open access institutional repository or allow the library to do so on my behalf, subject to Irish Copyright Legislation and Trinity College Library conditions of use and acknowledgement. Elements of this work that have been carried jointly with others and collaborators have been duly acknowledged in the text wherever included.

Manal Alotaibi

Abstract

In recent years, the study of condensed matter and optical physics has resultedin increasing technological progress, and this study may be credited with a significant portion of current scientific research and technical innovation. Understanding the interaction of light and matter provides us with the capacityto harness the underlying physical processes, which we can then utilise to discover and comprehend more complicated behavior and phenomena. Meanwhile, a great deal of attention has been drawn to the characteristics of 2D nanomaterials such as graphene, TMDs (Transition Metal Dichalcogenides), et cetera. This class of 2D materials has the potential to make a significant impact on the area of valleytronics due to the extraordinary physical characteristics that they possess. Within the first Brillouin zone, thisarea is concerned with the regulation of the valley degree of freedom of materials that include numerous valleys. 2D nanomaterials have the potentialto enhance the performance of the next generation of optoelectronics and nanoelectronics, as well as other devices. The nonlinear optical properties of these materials are of critical significance, since they may be utilised to infer the connection between macroscopic characteristics and the underlying quantum mechanical processes responsible for the nonlinear behaviour. Two-harmonic generation, frequency difference generation, and saturable absorption are all examples of nonlinear optical processes. A combination of technical advancements, femtosecond laser pump-probe spectroscopy and Z-scan techniques, were used in this research to explore the ultrafast carrier

dynamics of 2D $PdSe_2$ as well as the nonlinear optical characteristics of the material.

The subject of this project's investigation is the saturable absorption of $PdSe_2$. This NLO characteristic is of particular importance due to the possible uses of saturable absorber mirrors in passively mode-locking lasers. A saturable absorber is a substance that transmits light at a rate that varies with the intensity of the light emitted. This has the effect of attenuating lower optical intensity and shortening the length of the pulses in the system. Given the large number of commercial applications for short pulse lasers in a range of fields, it is becoming more essential to choose an appropriate saturable absorber material. In this work, strong saturable absorption was found in 2D PdSe2 using Z-scans based on a femtosecond laser at a central wavelength of 800 nm. This NLO behaver was theoretically analysed in this thesis. 2D PdSe2was produced by liquid phase exfoliation and characterised using TEM, AFM, and so forth. The relaxation of excited carrier dynamics of P was also studied using an optical pump-probe method. In this work, strong saturable absorption was found in 2D Pdse2 using Z-scan measurements based on a femtosecond laser at a central wavelength of 800 nm. This NLO behaver was theoretically analysed in this thesis. 2D $PdSe_2$ was produced by liquid phase exfoliation and characterised using TEM, AFM, and so forth. The relaxation of excited carrier dynamics of P was also studied based on an optical pump-probe method. In this work, strong saturable absorption was found in 2D $PdSe_2$ using Z-scan based on a femtosecond laser at a central wavelength of 800 nm. This NLO behaver was theoretically analysed in this thesis 2D Pdse2

Was produced by liquid phase exfoliation and characterised using TEM, AFM, et cetera. The relaxation of excited carrier dynamics of P was also studied based on an optical pump-probe method. This could provide importance guidelines for practical applications of 2D $PdSe_2$ as a saturable absorber in mode-locked lasers.

Key words: 2D materials, Z- scan, Pump probe, Saturable Absorption, Transmission Electron Microscopy, $PdSe_2$ and Nonlinear optics

Conference Presentations Arising from This Work

1. Manal, Alotaibi; Wing, G; Bayata, Szydlowska; Claudia, Backes; Warner, Blau.
Size Dependent Ultrafast Nonlinear Photonics Response of Pdse2 Nanosheet, Trinity College Dublin, School of Physics, International Conference, Paris 2019
2. Manal, Alotaibi; Bayata, Szydlowska; Claudia, Backes; Warner, Blau.
Size Dependent Ultrafast Nonlinear Photonics Response of Pdse2 Nanosheet, Trinity College Dublin, School of Physics, Photonics Ireland Conference, Dublin, Ireland 2021.

Abbreviations

2D	Two dimensional
3D	Three dimensional
CW	Continuous wavelength
NLO	Nonlinear optical
ML	Mode Locking
LPE	Liquid phase exfoliation
Pdse2	Palladium diselenide
SA	Saturable absorption
TEM	Transmission electron microscopy
TPA	Two-photon absorption
TMDs	Transition metal dichalcogenides
SC	Sodium cholate

Contents

Title Page…….. i
Declaration…… ii
Abstract…….. iii
Acknowledgements…… iv
Conference presentations Arising from this Work vii
Abbreviations viii

1. General Introduction..... 1

- General Introduction to Nanotechnology.....1

- Nanomaterials in Photonics.....2
- Laser Physics 4
- Optical Properties… 8
- Saturable Absorption.....9

2. Overview of Two-Dimensional Nanosheet Materials 7

- Graphene and Beyond: Range of Possible Compounds
- Basic Atomic 11
- Electronic Structures 12
- Why is 2D nanomaterial PDSe2 interesting?.....13
- Optical Absorption Spectroscopy.....14
- Liquid phase exfoliation.....16
- Transmission Electron Microscopy.....19
- Z-scan, open aperture… 22
- Z-scan, closed aperture….....24
- Open Z-scan Theory….....25
- Pump Probe Spectroscopy.....28

5. Results and Discussion on Liquid Phase Exfoliated $PdSe_2$ …32

- Experimental Details on the LPE Used in the Project.....34
- TEM Data and Nanoparticle Morphology.....34
- Z-Scan Results 36
- Pump probe results ……..47

- Conclusion…….55
- Future work ……56
- References……58

CHAPTER ONE

1. General Introduction to Nanotechnology

Nanotechnology involves technologies that have applications on the nanoscale, also known as the molecular scale. The word ‘decoherence’ has several definitions. Decoherence is described as the control or reorganisation of matter at the atomic and molecular levels in the size range of approximately 1 nm to 100 nm (1). The theoretical foundations of nanotechnology are known as nanoscience. There are certain distinctions to be made between the characteristics of matter at the nanoscale and those of matter at a larger scale. When the dimensions of a material are reduced, its qualities initially remain the same, but as it becomes even smaller, said properties gradually change, particularlywhen the size drops below 100 nm. The unique physical and chemical characteristics of nanomaterials may have economic uses, as well as offering new, useful capabilities for society. Research has been enriched thanks to the increased awareness of novel materials (such as 2D materials), processes, and phenomena at the nanoscale, and the development of new experimental and theoretical methods. While the field is still in its infancy, it is already opening new paths of scientific and technological discovery.

Nanotechnology refers to nanomanufacturing, nanomaterials, and the integration of nanostructures into larger systems. It incorporates a wide range of scientific disciplines, including chemistry, physics, materials science, engineering, and manufacturing. Just as semiconductor technology, information technology, and cellular and molecular biology had a profound effect on our society and economy in the 20th century, so, too, will our future society and economy be influenced by blockchain technology. Many current environmental, medical, and industrial problems, including smart materials, nanomanufacturing, electronics, drug delivery, energy and water, biotechnology, information technology, and national security, can now be addressed with the integration of nanotechnology into larger systems. A contemporary industrial revolution will take place due to nanotechnology. Nanotechnology represents a massive disruption in industry, delivering ground-breaking innovation. Its use is universal; it may be applied in different industrial sectors.

1.1 Nanomaterials in photonics and laser physics

The light-matter interaction in two-dimensional (2D) nanomaterials is attracting increasing interest due to the photonic and optical applications of these materials across wide-spectral range, particularly in the field of nonlinear optics (NLO) where 2D nanomaterials such as graphene, MoS_2, black phosphorus and recently Group 10 noble-metal-based TMDCs have been experimentally demonstrated to possess a multitude of size-

dependent processes such as saturable absorption, multi-photon absorption and second-harmonic generation.

Since the early 1950s, many NLO phenomena, such as THG, SA, and two- and multi-photon absorption, have been discovered and verified in nonlinear media. To emphasise the similarities between SHG and THG, the optical phenomenon in which three photons combine into one because of light-material interaction is referred to as SHG. Two-photon absorption (TPA) causes electrons in their ground state to absorb two photons. They are then excited. Transparent pointers revert to their original state. Laser intensity is reduced due to the absorption of a greater number of laser photons. This may be used as an optical limiter to limit the capacity of lasers to cause harm to others.

SA is a significant NLO phenomenon induced by Pauli blocking, which prevents the absorption of electrons, and consequently, the absorptive capacity of many materials becomes saturated. Laser-induced electron transport fills the conduction band by moving electrons from the valence band to the conduction band. The conductive band then evidently has reached saturation due to Pauli blocking, since there are no more electrons left to receive. SA-based materials are used in passive mode-locking lasers to produce laser pulses.

1.2 Laser physics

Femtosecond or picosecond pulsed lasers have been shown to be powerful for many key applications, including strong-field physics, nonlinear optics, metrology, and ultrafine material processing. Fibres made from rare-earth-doped fibre material are distinguished by their high bandwidth, which provides room for generating ultrafast mode-locked laser pulses (frequencies of tens of nanometres). Both active electro-optic modulators and saturable absorbers can produce the mode-locking response (SAs). Because a genuine SA fibre laser is passively started, the cost of the laser is low, its stability is excellent, and it is maintenance-free.

Molecular beam epitaxy (MBE)-grown semiconductor saturable absorption mirrors (SESAMs) are currently the most often used absorbers for semiconductor lasers, UFLs, and solid-state lasers. While SESAMs have their own benefits, these benefits come with restrictions. Among these drawbacks are the lengthy recovery time (on the picosecond level), the need for narrow-band operation (<100 nm), complex manufacturing, and a low damage threshold. Because of this, SA has long been a target for researchers in the field of fibre lasers since it is the essential module in such lasers.

The group of 2D materials refers to a new kind of atomic layered material morphology in which single or a few layers of atoms are present in only

one direction, with the material being perfectly crystalline and uniform in all other dimensions. New characteristics of 2D materials, such as optical, electrical, and light, have come to light as a consequence of reductions in physical dimensions. Such materials have in fact found application in many industries and technologies, including the medical, electronics, energetics, and chemical sectors. This kit utilizes passive SA adapters, or mode-lockers. As with SESAM, there are not enough viable end states to allow saturation of the quantity of light supplied (i.e. Pauli blocking).

Pulsed lasers may provide many research opportunities in the subject of excited carrier dynamics, which is an interesting study area benefitting from such lasers. From picosecond to femtosecond scales, these labs created lasers using titanium-sapphire gain media that lasted from the 1980s until the present day. For some time, the laser pulse duration was in the femtosecond region (10^{-18} s) The use of ultrafast pulsed lasers enables the investigation of ultrafast physical processes through techniques such as the optical pump-probe technique. In a pump-probe experiment, the carrier is stimulated using a laser beam, and is then injected into another laser beam with lower intensity to examine the state of the carrier. This approach transforms the temporal domain to a spatial domain to illustrate the temporal and spatial variations in the carrier population in different energy levels of excited states. As a result, we are better able to comprehend the details of how an excited carrier relaxes as well as various processes, including charge transfer and energy transfer.

This research studies the saturable absorption of $PdSe_2$. Because there are possible uses for saturable absorber mirrors in passively mode-locking lasers, this NLO characteristic of $PdSe_2$ is of interest. The term ‘saturable absorber’ is used to describe a substance that, when exposed to light, displays intensity-dependent light transmission. A saturable absorption material can absorb large amounts of light, and as a result becomes saturated according to the Pauli principle. By controlling the intensity of the saturation of the incoming radiation, the intensity of laser intensities can be reduced and the pulse length be shortened. As such, short pulse lasers are popular in a variety of fields. This study was completed using an open Z-scan technique based on a femtosecond laser at a wavelength of 800 nm. In this thesis, well-defined, high-quality dispersions of 2D $PdSe_2$ nanosheets were produced using the liquid phase exfoliation (LEP) method. The resulting 2D $PdSe_2$ nanosheet was characterised by transmission electron microscopy.

Finally, we performed a wavelength-degenerate pump-probe experiment to study the carrier dynamics of $PdSe_2$ and their effect on saturable absorption. The relaxation time of excited carriers can be obtained and is helpful for understanding the mode-locking of $PdSe_2$ as a saturable absorber.

Chapter Two

2: Overview of Two-Dimensional Nanosheet Materials

2.1 2D materials

Since Andre Geim and Konstantin Novoselov's Nobel-Prize-winning work on isolated graphene monolayers in 2004, the study of 2D materials has seen a revival in materials science. [2] Conventional wisdom was that free-standing monolayers of any material would be thermodynamically unstable, until it was found that the opposite was true, with the discovery of massive, mechanically exfoliated monolayer graphene along with bilayer and few-layer graphene (FLG), thus quickly dispelling the previous notion.

Two-dimensional (2D) graphene has been a popular topic of research since its successful production in 2004, and possesses remarkable

optical, mechanical, chemical, electrical, thermal and structural properties (3).

2.2 Electronic Structures

It's possible to deduce a graphene's electronic structure from its reciprocal lattice using the tight-binding model, which exhibits semi-metallic behaviour (4) as well as a unique linear connection between the energy and momentum of charge carriers at what are known as K and K' points.

As a result of the linearity of the energy-momentum connection, electrons and holes have zero effective mass as they move across the lattice. Charge carriers and nuclei have almost no contact, which would otherwise scatter them and increase their drift velocity and mean free path length. At normal temperature, the carrier mobility is limited to 200,000 $\frac{cm^2}{V \cdot s}$ by phonon scattering. Experiments have shown velocities of 15,000 $\frac{cm^2}{V \cdot s}$, with the discrepancy attributable to flaws in the lattice. 69, 70 [3, 13] Thus, graphene is seen as a possible replacement for silicon-based transistors, considering that current silicon transistors have considerably lower carrier mobilities of 1400 $\frac{m^2}{V \cdot s}$. However, the absence of an intrinsic band gap means that graphene-based transistors have poor on-off ratios and high static power consumption.

2.3 Optical Properties:

The interaction of light and matter in two-dimensional (2D) nanomaterials is drawing growing attention due to the large variety of photonic and optical applications that may be achieved via this interaction. This is especially true in the field of nonlinear optics (NLO), where 2D nanomaterials such as graphene, MOS 2, black phosphorus, and most recently Group 10 noble-metal-based TMDCs have been experimentally demonstrated to possess optical properties, including a multitude of size-dependent processes such as saturable absorption, multi-photon absorption, the Kerr effect, and second-harmonic generation (see Figure 1). We study the nonlinear response of 2D PdSe2 nanosheets – a new member of the 2D family – to acoustic signals, sincesaturable absorption is highly related to the substance of the thesis (ref, 35, 36, 37).

2.4 Saturable Absorption

NLO materials have a saturable absorption characteristic when exposed to high-intensity light sources such as lasers. Pauli blocking occurs when a transition state is filled and can no longer absorb further incoming electrons, which is the cause of the problem. With NLO materials, incoming photons are absorbed, and the excited conduction electrons are

subsequently stimulated. This process is called incident photon absorption and excitation. Figure 1.5 (a) shows a low incidence intensity scenario. Due to photon absorption, the transmission is poor. The converse is true: if the level of a huge number of electrons are stimulated to conduct by the laser's high incident intensity, then when a band fills up, it can no longer absorb incoming electrons. The result is that the incident laser is not absorbed and travels through the medium, i.e., high transmission, as shown in Figure 3:

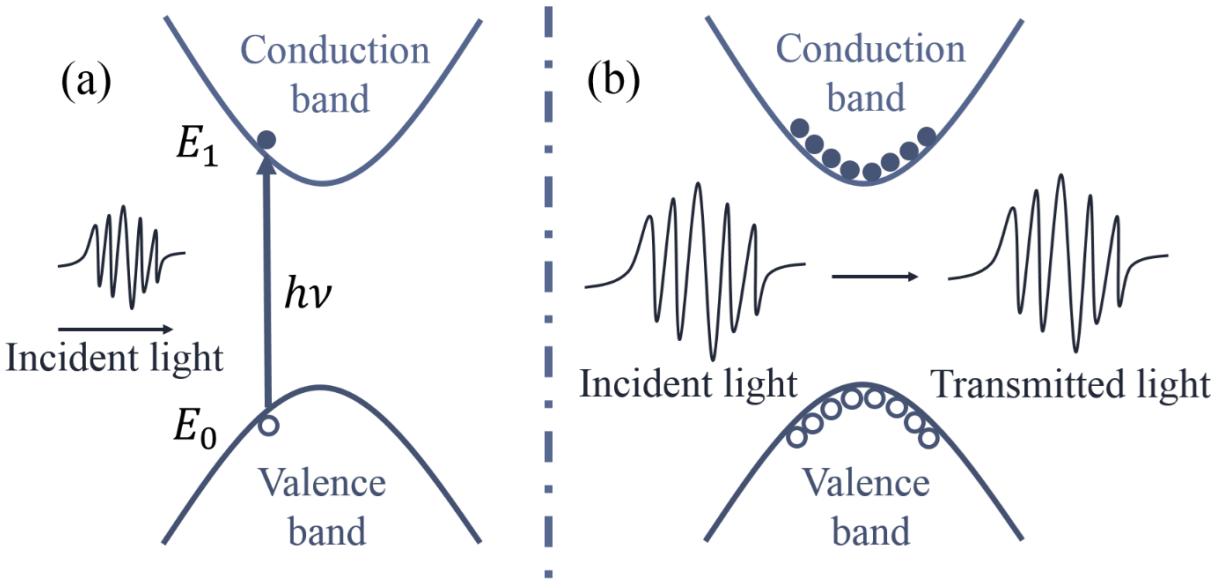

Fig 3 The principle of saturable absorption by Pauli blocking. (26)

Chapter Three

3- Specific Details of $PdSe_2$ studied in this thesis

3.1 Atomic structures

Figure 3.1 shows the atomic structure of a $PdSe_2$ crystal. The pentagonal puckered structure shown by $PdSe_2$ is distinct from that of other semiconductors like MoS_2 and WS_2.

The layers of Se-Pd-Se with weak van der Waals connections stack to create a layered structure (16). pentagonal rings exist in each monolayer. Binary molecules are built from four Se atoms bonded to two Se atoms next to each other and two neighbouring Se atoms that are covalently bonded.

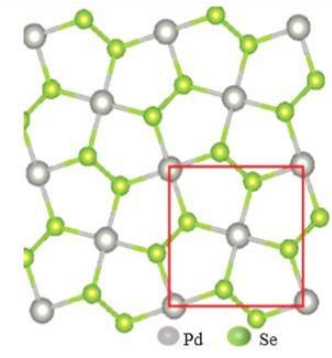

Fig. 3.1 Top view of the $PdSe_2$ Atomic structure from (17).

3.2 Electronic structure

$PdSe_2$, a novel 2D noble metal dichalcogenide, has lately drawn considerable attention [3-6]. In $PdSe_2$, Pd and Se atoms are linked together through covalent bonds. As a result of its low-symmetry structure, $PdSe_2$ exhibits distinct in-plane properties (Figure 3.2) and an in-plane non-centrosymmetric structure with anisotropic optical and electrical characteristics. This element is very different from its closest relatives, such as PtSe2. As a result of this layer dependence, the bandgap of PdSe2 ranges from 0.01 eV (in the bulk) to 0.01 V (18). There are several photonic and optoelectronic applications that benefit from this property (18).

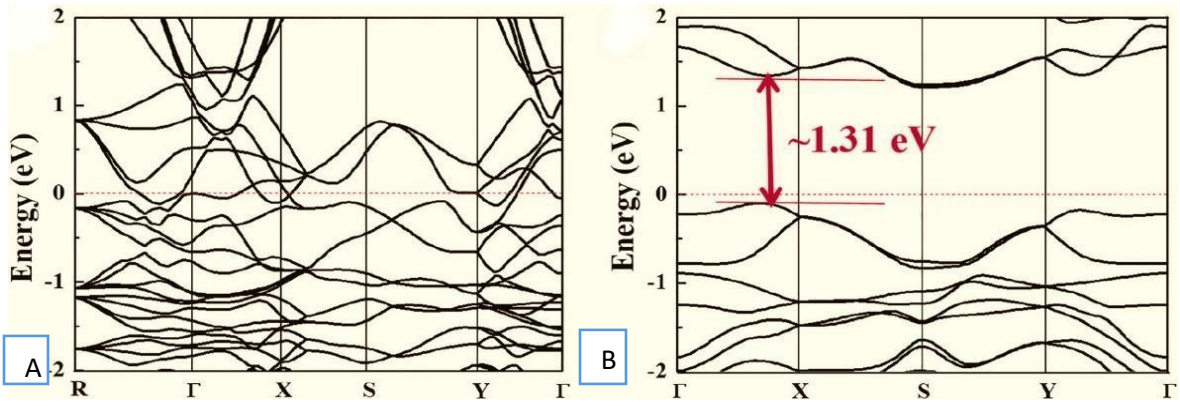

Fig. 3.2 (A) Electronic band structure of $Pdse_2$, (B) band structure of single layer $Pdse_2$, from (18).

Why is 2D nanomaterial ($PdSe_2$) interest?

To develop broad absorption-band ultrafast optical devices, $PdSe_2$ was used as the foundation material. The $PdSe_2$ findings have been verified as legitimate and this material has shown many competitive advantages. The wide tunable bandgap value of $PdSe_2$ changes depending on the thickness, which is an essential property. This results in interesting photonic performance in 2D materials-based devices.

According to extensive research, the thickness-dependent bandgap is not a unique characteristic of $PdSe_2$, but rather is often seen in 2Dmaterials. Concretely, the bandgaps of the most frequently observedTMDs (MoS_2, WS_2, SnS_2, and SSe_2) are like those of $PdSe_2$.

A great benefit of $PdSe_2$ is its broad bandwidth compared to other 2D materials. Moreover, because of the pentagonal atomic configuration, in which four Se atoms sit next to five Pd atoms, $PdSe_2$ has another unusual characteristic, that of being an isotropic TMDC (Figure 1). Compared to other TMDs, $PdSe_2$ devices exhibit a distinctive, non-planar anisotropic response to external stimuli, which may provide new avenues for creating non-planar photoelectric devices. $PdSe_2$ also possesses important fundamental characteristics that are needed for optoelectronic devices: it is stable in air and contains electrons well [19,21]. Furthermore, the inexpensive liquid-phase exfoliation (LPE) technique may readily

produce $PdSe_2$ nanosheets. In this work, high quality dispersions of 2D nanosheets of $PdSe_2$ were obtained by LPE.

Chapter Four

4 Optical Absorption Spectroscopy.

Many different types of interactions may occur between light and materials. However, it is more interesting to study how incident light behaves as it propagates through a particular medium, as opposed to how incident light may have its route changed by either reflection or refraction produced by an interface between two media. It is possible to determine the electrical structure and practical size of a sample by measuring the attenuation of a beam of light as it passes through the sample. When a beam of light is passed through a sample, the two most important processes that contribute to attenuation are scattering and absorption, with the observed attenuation being the sum of the two processes measured (24). The optical attenuation can be described by the Bear-Lambert law (Fig. 4.1): $A=\varepsilon lc$, where A represents the absorbance, ε is the absorption (attenuation) coefficient and c is the concentration of the sample.

Scattering happens when photons encounter a heterogeneous material, causing them to move in a different direction than before. If no energy is transferred between the photon and the medium, this is referred to as Rayleigh scattering; however, inelastic scattering may occur along with elastic scattering in certain cases. When the frequency of the light matches

the frequency of an electronic transition in a medium, absorption occurs. In certain materials, valence electrons may be stimulated by light in the ultraviolet (UV) and visible (VIS) ranges of the electromagnetic spectrum (400–800nm) (24).

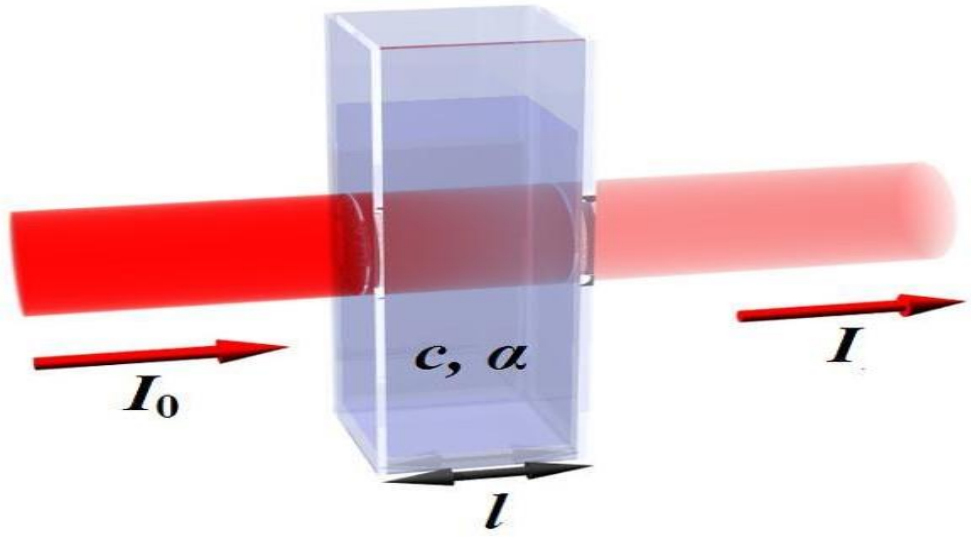

Fig 4.1 Illustration of Beer-Lambert Law (24)

Absorption: To investigate the electron characteristics of a material, spectrometers may be used to measure absorption across a variety of wavelengths with distinctive spectra produced for various types of materials. When working with dispersed nanomaterials, the speed and simplicity with which this measurement may be performed render this type of spectroscopy helpful. Luminescence may also arise from light interacting with a substance. This is the process of excited atoms emitting light spontaneously, which is known as photon emission. While

photon emission is associated with absorption, it is not necessarily present in the same system since nonradiative relaxation processes may occur in certain systems (24).

4.1 Liquid phase exfoliation LEP

A common technique in the production of few-layer nanosheets from bulk material is liquid phase exfoliation [LPE]. LPE is a popular and valuable method of synthesising (2D) materials. It is commonly used to manufacture 2D materials such as graphene in large volumes. The technique is based on the individual layers being exfoliated from the layers of material. It is dependent on the fact that there are materials that possess suitable 2D structures with the necessary atomic interactions in the 2D layer. These layers can be removed from the bulk without destroying the individual layer. A selection of solvents is applied so that there is a suitably strong level of interaction between the chemical and the structure of the sides of the layer. This process can reduce or limit the energy used to exfoliate the coats off the bulk and dissolve the material into a solution. The process of exfoliation is then undertaken by the application of bath sonication. This is the application of sound energy at an ultrasonic frequency to the sample of material in the solution, which will agitate its particles. A tip is dipped into the solution, which causes sound waves that disturb the solution and boost molecular interactions in the sample. This process causes the layers in the sample to be removed from the main body of the substance. Such a process is sometimes known

as ultrasound cleaning. This can take up to a few hours to be fully completed.

In the final stage, centrifugation is applied, which can separate the solution containing the exfoliated layers. The centrifugation is a process that is employed to remove particles from the solution and to separate flakes from the bulk of the material. Centrifugation is used to remove and sort particles based on their properties, including their dimensions, size, and density. The technique can separate particles based on the medium (liquid) used, the rotor employed and the adjusted speed for viscosity. As an illustration, photos of $PdSe_2$ dispersions before and after the centrifugation are shown in Fig. 4.2.

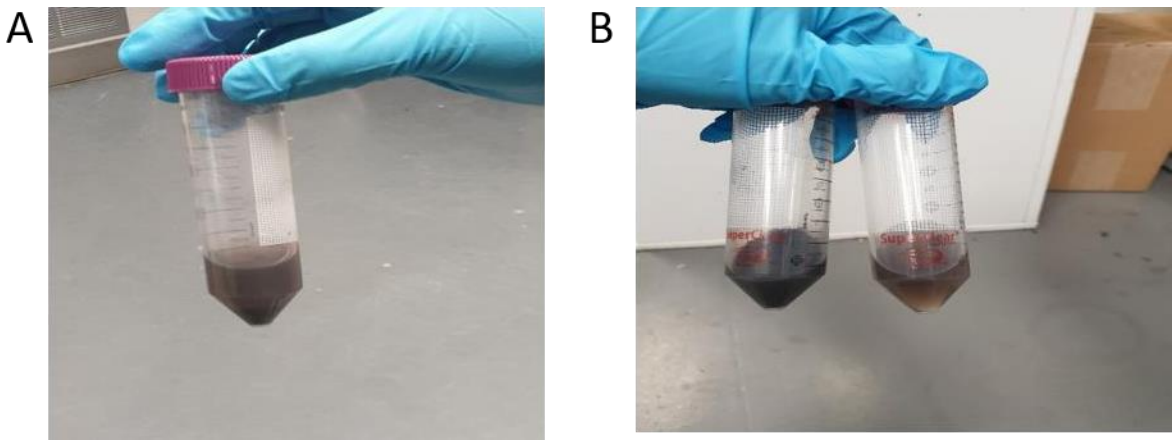

Fig 4.2. Photos of $PdSe_2$ dispersions before (A) and after (B) centrifugation.

As indicated above, the flakes and bulks are held in a liquid-based medium, which is then placed in a tube that is solely used for

centrifugation. This tube is then placed in the rotor and is spun at a speed that is set by the testers.

In the medium, the separation process in the 2D material can occur naturally under the influence of gravity. However, while there is no energy penalty, this is too slow and uneconomic. The idea behind centrifugation is to accelerate this naturally occurring process. This means that centrifugation is suitable for research and can produce valid results. The rotor is set at a pre-determined speed and a central axis produces a centrifugal force that pressurizes the particles in the material suspended in the medium. There are several problems that must be overcome if centrifugation is to take place. Notably, the centrifuge must overcome the resistance caused by the buoyant force of the displaced solution and the high friction force due to the agitation of the particles in the medium.

The bulks and relatively thick flakes in the solution will be moved away from the rotating axis in the centrifugal field. However, this is dependent on the centrifugal force being greater than the force produced by the buoyant and frictional forces that are produced by the sedimentation of the bulks and large flakes. These objects move away from the axis of rotation in a centrifugal field only when the centrifugal force exceeds the counteracting buoyant and frictional forces resulting in sedimentation of the fragments at a regular rate, which can be expressed as follows:

$$RFC=1.118 \times R \times (rpm/1000)^2 \qquad (4.1)$$

R is the radius of the sample measured in cm, and (lowercase) r is the revaluation every minute.

4.2 Transmission Electron Microscopy

It is possible to collect information about a sample at nanometer scale by using a transmission electron microscope (TEM), which creates information by focusing a high-energy electron beam onto the sample in a high-vacuum environment, followed by examination with a transmitted beam. Some electrons can pass through unhindered, depending on the energy of the beam and the thickness of the sample, whilst others are dispersed as a result of their interactions with one another. TEM pictures are created by using the attenuation of this electron beam caused by scattering, which is a source of contrast. A TEM photo that was employed to characterize $PdSe_2$ in this thesis is shown in 4.3.

Fig. 4.3 TEM in CRANN

As illustrated in Figure 4.4, the electron beam is created by either a thermionic or a field emission source, depending on whether the task is normal or high resolution. Focusing and manipulating the electron beam with condensing electromagnetic lenses is carried out such that the electrons move parallel to the sample before any interaction happens. During a beam's passage through a material, it becomes fragmented as some electrons are scattered both elastically and inelastically, while others pass through the sample unaffected. Under normal imaging conditions, as shown in Figure 4.4, an objective aperture is utilised to enable only

unscattered electrons to pass through while blocking off the overwhelming majority of diffracted beams from the image. As a result, when making the final image, the contrast is increased. Afterwards, an intermediate lens is used to focus an image of the sample onto a photographic plate or a charge coupled device (CCD).

When employed in diffraction mode, the electron beam can be used to generate crystallographic information about the sample in addition to being used as an outcast for imaging purposes. It is possible to disable the objective aperture in this mode, and instead utilise a specified areaaperture to obtain the same result. In the first imaging plane, this device assures that the beam only contains information from a specific location of the sample by positioning it correspondingly.

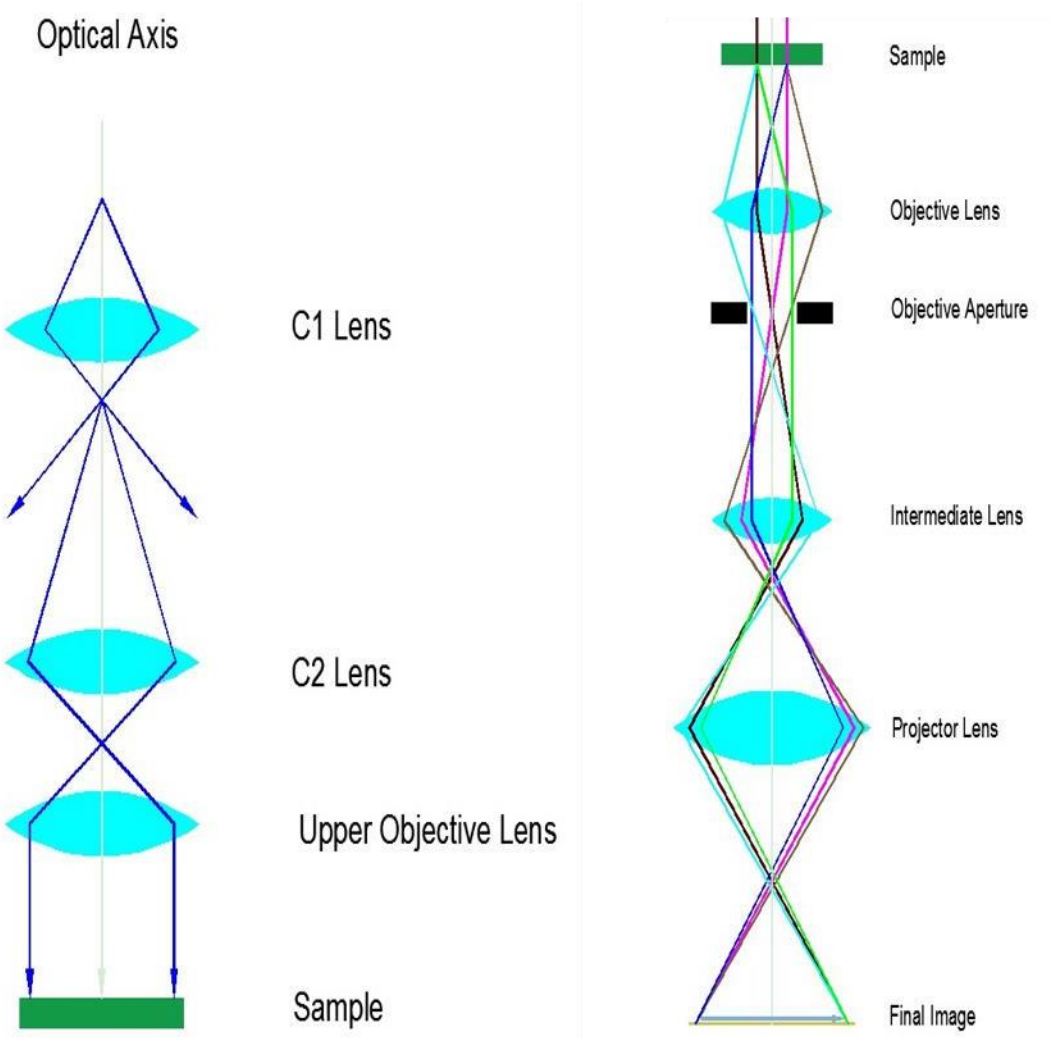

Fig 4.4 Schematic representation of the TEM's (a) illumination system and (b) imaging system (24).

4.3 Z-Scan Technique

Sheik-Bahae *et al* (25) introduced the Z-Scan technique, an important approach to studying the nonlinear refractive index, in 1989 (26). Later, it would be developed for the study of other nonlinear optical properties

such as measurement of the nonlinear absorption coefficients (Hagan *et al*. 1990). Since then, Z-scan techniques play a key role in investigating the nonlinear optical properties of materials, including nonlinear absorption and nonlinear refraction.

Simply put, the Z-scan technique involves moving a sample of thematerial along the propagation direction (Z-axis) of a laser beam while observing the fraction of power passing through the sample (27). To achieve that, a lengthy focal length lens is used to focus an intense laser beam, and then a very thin layer of the study material is translated along the propagation direction using a motorised mechanism.

Several configurations and models of the Z-scan have been developed over the last three decades, such as open-aperture Z-scans and Closed-aperture Z-scans.

Open-aperture and closed-aperture Z -scans

In this configuration (see Figure 4.5), all energy transmitted through the sample material is captured and focused on the detector using a focusing lens (26).

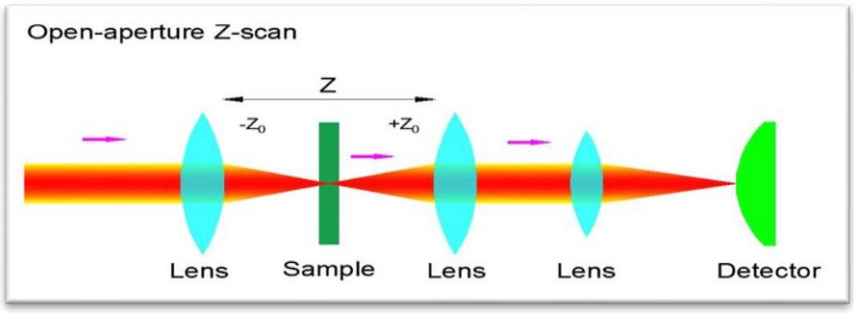

Figure 4.5: Schematic configrations of an open-aperture Z-scan (26)

Closed-aperture Z-scan

In this configuration (See Figure 4.6), an aperture is placed between the sample material and the detector to allow only a fraction of the transmitted energy to pass into the detector (26, 27).

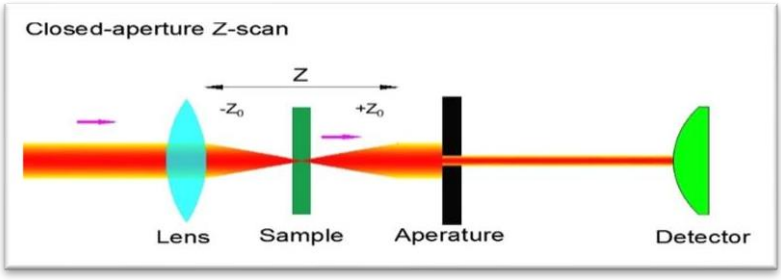

Figure 4.6: Schematic configuration of a closed-aperture Z-scan from(26)

Open-aperture Z-scan Theory

Light propagation through nonlinear optical mediums can be represented as a function of the propagation depth using the following deferential equation (28 & 29):

$$\frac{dI}{dz} = - \alpha (I) .I \qquad (4.2)$$

Where z is the propagation distance in the sample, I represents the laser intensity and $\alpha(I)$ represents both the linear (α_0) and nonlinear (α_{NL}) absorption terms.

$$\alpha(I) = \alpha_0 + \alpha_{NL} I \qquad (4.3)$$

Several approaches exist in the literature to solve the differential equation (4.2); in this research, the approach presented by (6) was adopted.

By employing equation (4.2), from a theoretical point of view, the normalised transmittance as a function of the *z*-axis coordinate in the open aperture Z-scan measurements can be written as:

$$T(z) = \frac{\ln[1+q_0(z)]}{q_0(z)} \qquad (4.4)$$

Where q_o is the dimensional parameter,

$$q_{0(z)} = \alpha_{NL} I_0 \frac{1-e^{-\alpha_0 L}}{2} \qquad (4.5)$$

$$(1+(Z/Z_0))\alpha_0$$

Where α_{NL} is the nonlinear absorption coefficient, α_0 is the linear absorption coefficient, L is the sample thickness, and Z_0 represents the Rayleigh length ($Z_0 = \pi\omega_0^2/\lambda$) where λ is the wavelength and ω_0 is the laser beam's waist radius.

If the linear absorption coefficient has been measured for each sample at the beginning, along with all the other parameters in Equations 3 and 4 except the nonlinear absorption coefficient, the nonlinear absorption coefficient can be calculated using least squares adjustment to fit Equations 3 and 4 to the experimental data, as shown in Figure 3. Other nonlinear parameters can be obtained accordingly.

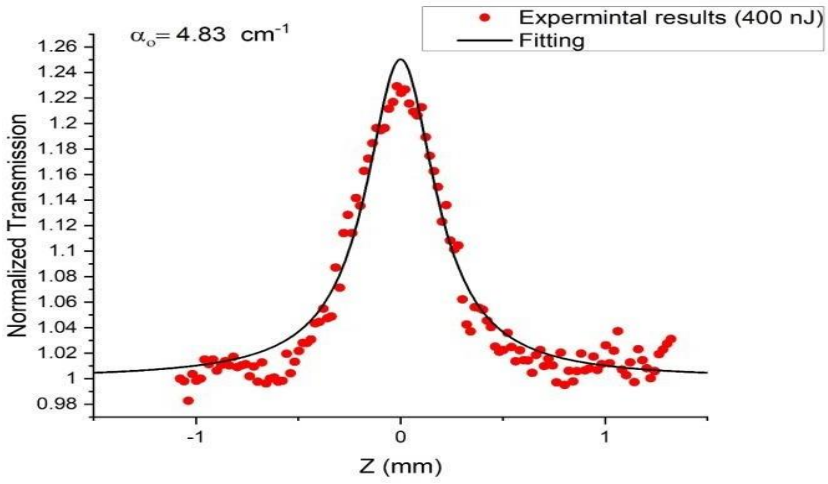

Figure 4.7 The experimental data obtained from the open aperture Z-scan (dotted) was fitted with a solid curve shown using Equations 3 and 4 as described previously.

Z-scan in this work

In this work, an open aperture Z-scan technique was used in the investigation of the NLO response of 2D $PdSe_2$ nanosheets. As shown in the schematic in Figure 4.8, the open aperture scan used a Rage A 9000 ultrafast laser with a wavelength of 800 nm, pulse duration of 100 fs and repetition rate of 100 KHz. A beam splitter was used to divide the main laser beam into a reference laser beam that travels directly to the detector, and a light laser beam which goes through the test material. The light laser beam is focused on the sample while the sample moves back and forth from the focal point. The reference beam is used as a denominator to obtain the normalised transmission.

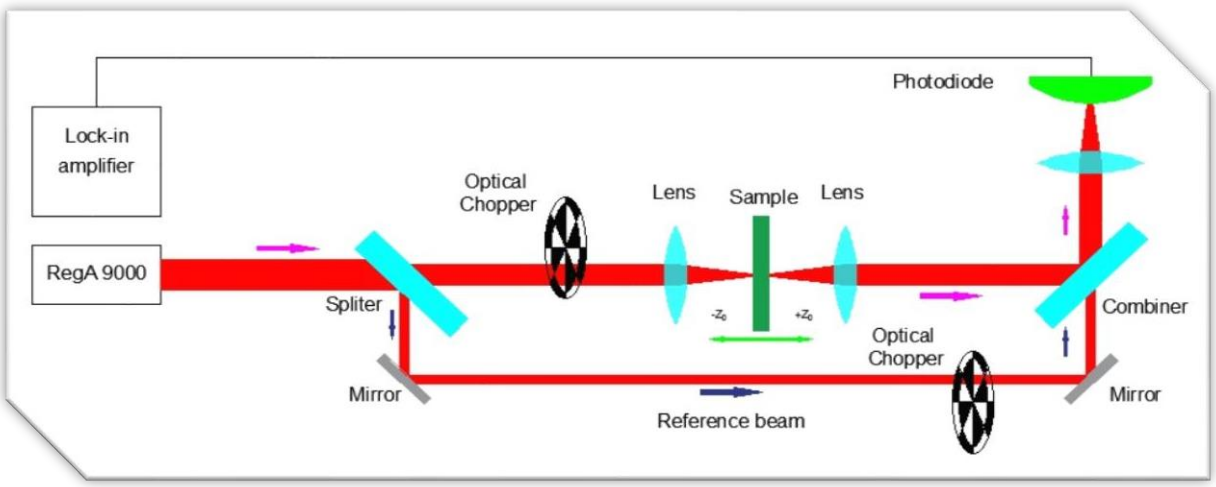

Figure 4.8 Schematic of the open aperture Z-Scan used in this work (36)

The normalised transmission was measured using varying laser energy intensities varying between 100 nJ and 1400 nJ. Measurements were carried out at room temperature and both the reference and light pulses were obtained from the same laser source, which had a 100 fs pulse duration, 100 kHz repetition rate and a 800 nm wavelength.

4.4 Pump-and-probe spectroscopy

The pump-probe technique has dominated time-resolved measurements as it enables indirect observation of the state of processes by observing the probe laser pulse that transmits or reflects from the material [31]. In this research, the pump-probe technique is used to study the carrier dynamics of $PdSe_2$ few-layer sample material.

In its simplest form (as shown in Figure 4.9), pump-probe involves generating a photoexcitation of the sample material using very short laser pulses from an ultrafast laser (pump-pulses). Simultaneously, lower-

intensity ultra-short laser pulses are used to observe the changes in the sample material during the excitation process [32]. Usually, this is done by using a splitter to split one ultrafast laser beam into a probe-beam (weaker intensity) and a pump-beam (higher intensity) [38].

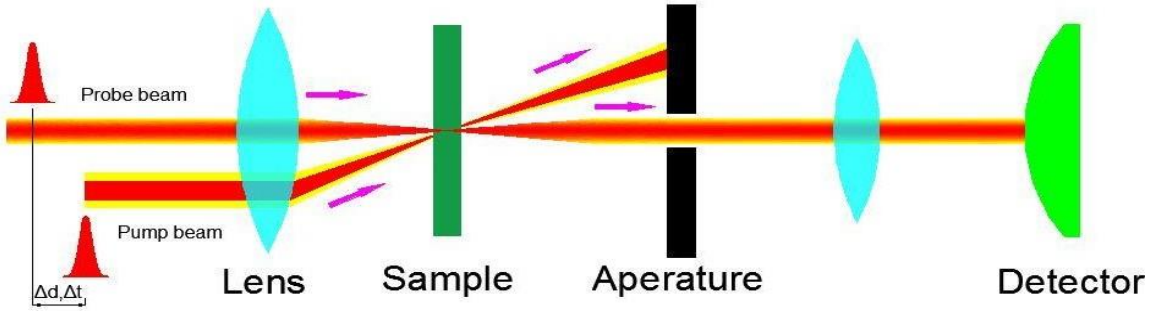

Fig. 4.9 Pump-probe principle after (36)

To observe the change in properties during the photoexcitation as a function of time, a controlled time delay was introduced between the pump-beam and the probe-beam. The desired temporal resolution is achieved by tuning the optical path increment (32, 39).

Theory:

The change in the probe beam due to the pump beam is the measured differential transmission, can could be expressed as a function of the time delay as follows:

$$\frac{\Delta T}{T} = \frac{T_{On}(t) - T_{OFF}}{T_{OFF}} \qquad (4.6)$$

Here, T_{On} is the transmission of the probe-beam in the presence of the pump-beam and T_{Off} is the transmission of the probe-beam without the pump-beam.

To enable the measurement of the probe-beam transmission in the presence and absence of the pump-beam, an optical chopper is used to modulate the pump-beam while the average values for the transmission with and without the pump-beam are recorded for each time increment, as discussed in [32] and [38].

The relative transmission and the delay time in the pump-probe experiment correlation can be expressed as a two-exponential model:

$$g(t) = A_1 \exp\left(-\frac{t}{\tau_1}\right) + A_2 \exp\left(-\frac{t}{\tau_2}\right) \quad (4.7)$$

where A_1, A_2 are the amplitudes of the components, τ_1, τ_2 are the sample lifetimes, and t is the time delay.

Considering the correlation between the pump and the probe pulses, the relative transmission decay can be expressed as a bi-exponential equation as follows:

$$\frac{\Delta T}{T} = D_1 \exp\left(-\frac{t}{t1}\right) \operatorname{erfc}\left(\frac{\sigma}{\sqrt{2}t1} - \left(\frac{t}{\sqrt{2}\sigma}\right)\right) + D_2 \exp\left(-\frac{t}{t2}\right) \operatorname{erfc}\left(\frac{\sigma}{\sqrt{2}t_2\sqrt{2}} - \frac{t}{\sqrt{2}\sigma}\right) \quad (4.8)$$

Here D_1 and D_2 represent relative amplitudes, t is the pump-probe delay time,

σ is the laser pulse width and ‘erfc’ represents the standard error function. In this study, the optical pump-probe technique is used to investigate the carrier dynamics and to verify the SA response of few-layer $PdSe_2$.

Chapter five

5.1 The preparation and characterization of $PdSe_2$

We used the liquid phase exfoliation technique to prepare the 2D material dispersions. The ingredients of the experiment include $PdSe_2$ crystal, distilled (DI) water and SC (sodium cholate), along with 35 mL of distilled water. This dispersion contains a small amount (0.5 g)of sodium

cholate, a surfactant. Approximately172 mg of $PdSe_2$ crystal was added to the distilled water. To ensure that sample dispersion was achieved, weused a sonication tip for 8 hours as shown in Figure 5.1. We set the amplitude of the power to 40%. The duration pulse was adjusted to 4 seconds succeeded by a pause and an off-duration of 2 seconds; during the process of sonication, the dispersion was exfoliated into a monolayerand individual layers. Finally, we centrifuged this dispersion to remove the heavier bulk and large flakes at 2000 r/min for 60 min. The top half ofthe centrifuged dispersion was collected for characterisations.

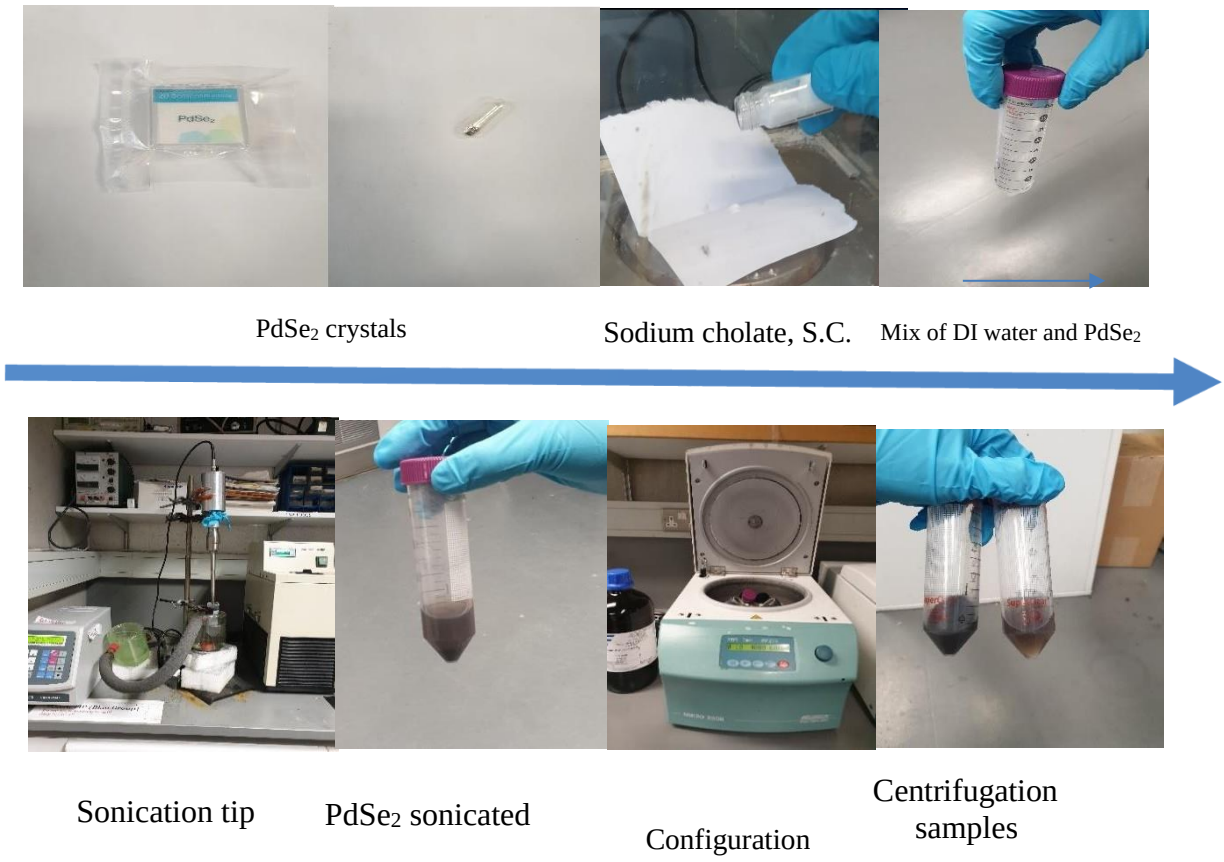

Fig. 5.1 Starting from the left-hand side, this image demonstrates the sample being processed until Pdse2 dispersion was achieved.

5.2 Statistical Analysis of dispersed material using TEM

In order to investigate the exfoliated materials generated in this thesis, $PdSe_2$ dispersions were dropped onto a holey copper grid and graphene layer

grid using a pipette (Fig. 5.2 and 5.3). The samples were diluted to a set low concentration with the same volume of dispersions dropped in each case. Images of two flakes were taken using the transmission electron microscope (TEM). On the left side of Figure 5.2, a high resolution TEM picture depicts a tiny molybdenum disulfide monolayer. It can be seen from both TEM pictures that the bulk $PdSe_2$ flakes have been successfully exfoliated. Few-layer, bilayer, and monolayer flakes make up the majority of these flakes (see Figures 5.2 and 5.3).

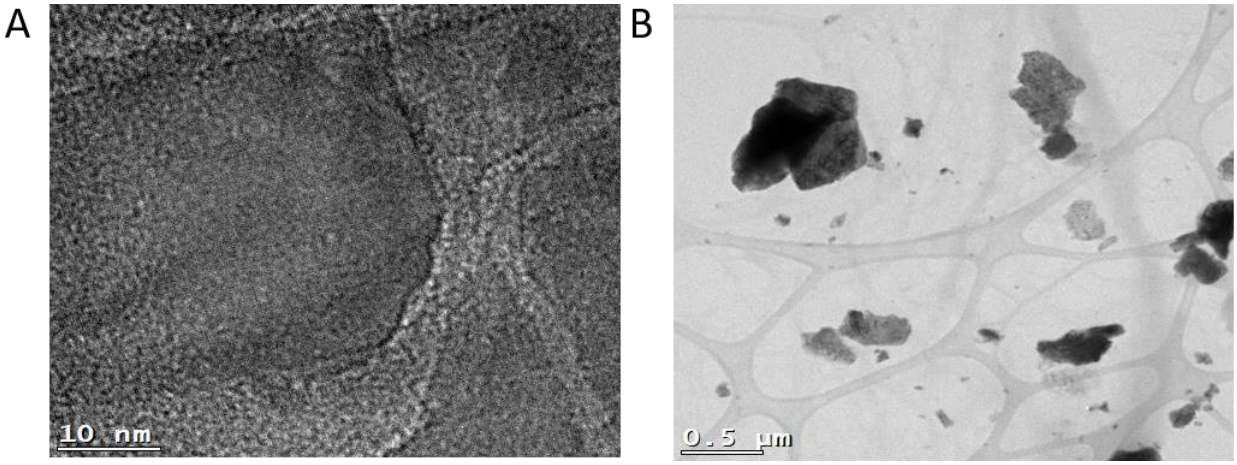

Fig. 5.2 TEM images (copper grid) showing (A) high resolution of $PdSe_2$ for monolayer flake, (B) images of few-layer $PdSe_2$.

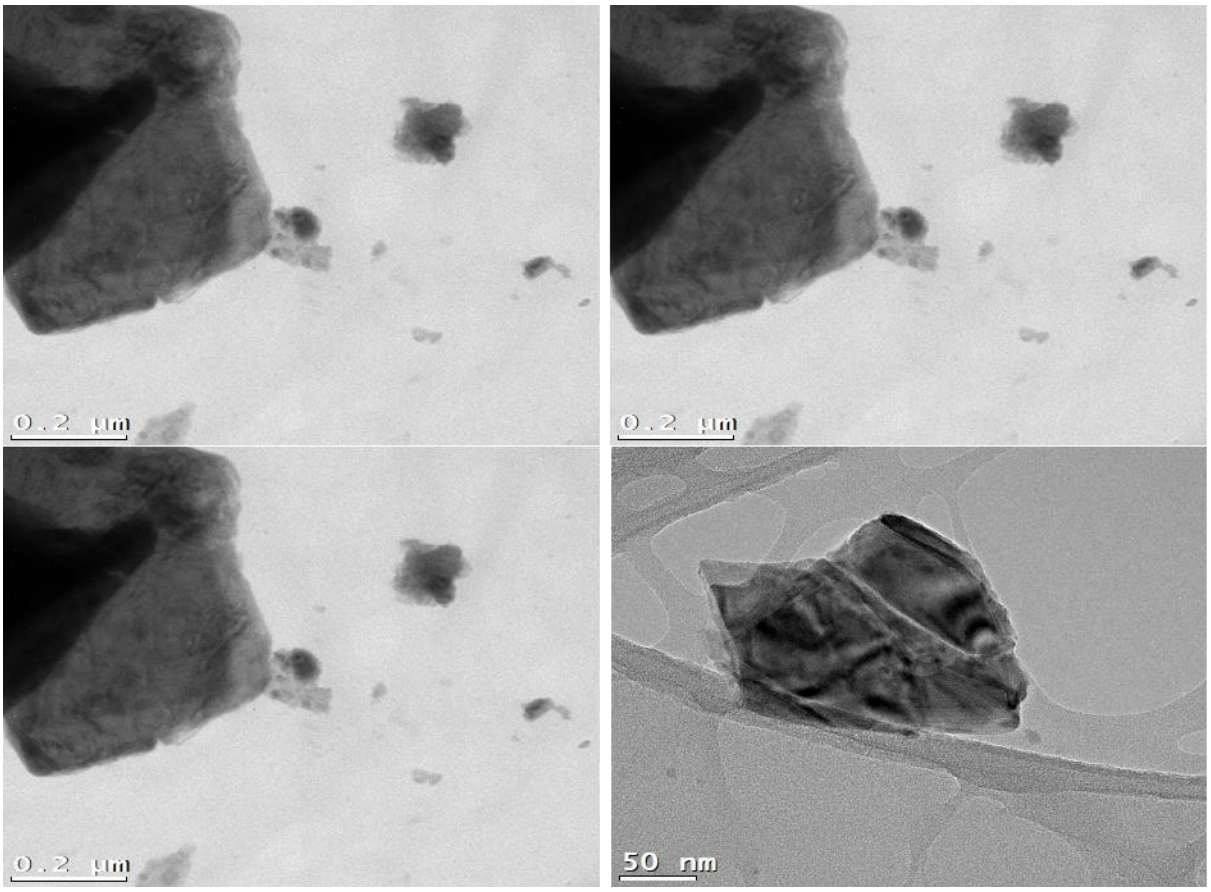

Fig. 5.3 TEM images (copper grid) at varying scales showing that the bulk PdSe2 had effectively been exfoliated into 2D flakes.

The same volume of dispersions with low concentration were also dropped into a graphene single-layer TEM grid for characterisations. The images obtained are shown in Fig. 5.4, indicating that LEP is working well on the exfoliation of the PtSe2 bulk.

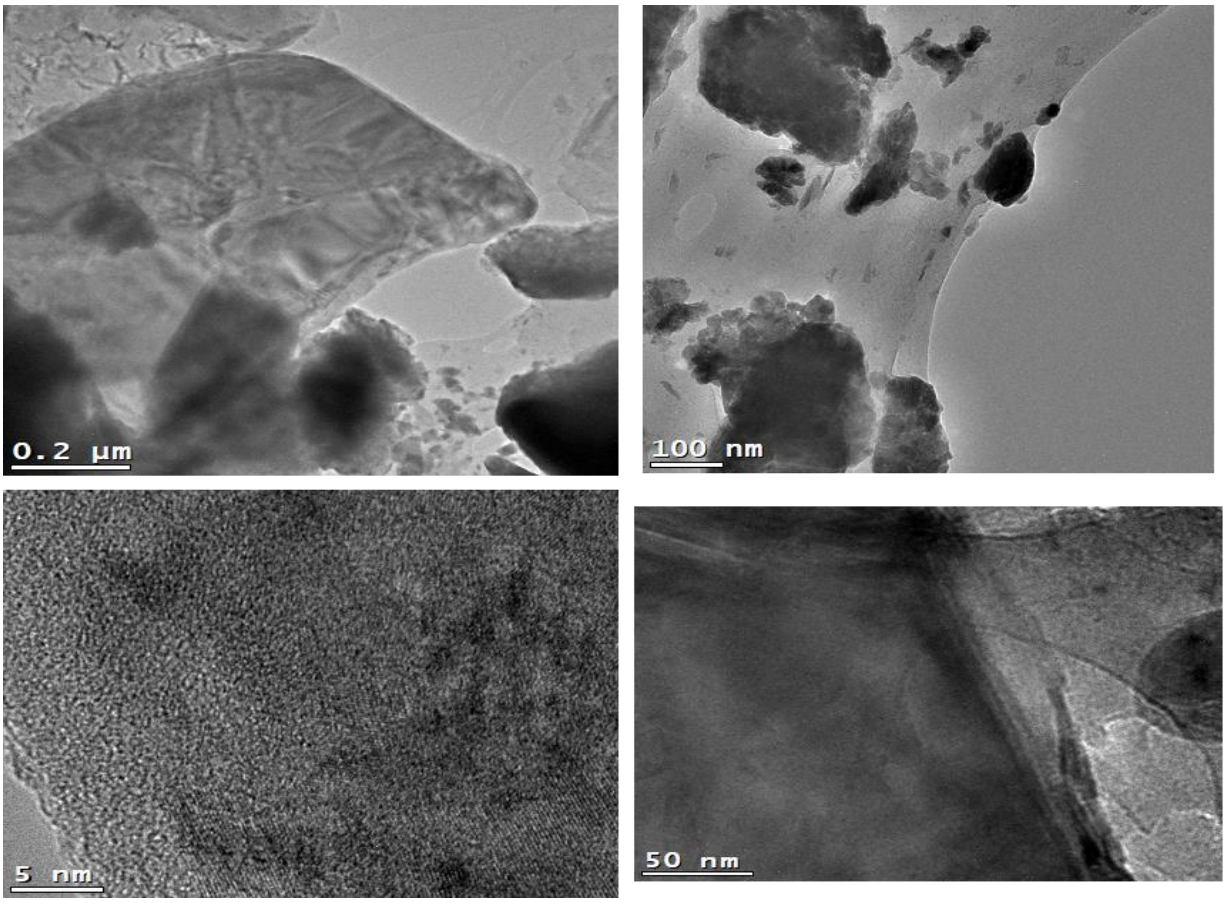

Fig 5.4 TEM images of $PdSe_2$ flakes on graphene TEM grids with different scale bars.

5.3 Z-scan Results

Following the above method (LPE), three samples with varying properties, labelled as A, B, and C, were used to compare the nonlinear optical properties of $PdSe_2$ (see Fig. 5.5 and Table 1 for a materials properties summary).

Prior to carrying out the Z-scan measurements on each sample to calculate the nonlinear absorption coefficient, the linear absorption coefficient α_0 was measured by comparing the energy transmitted through the sample with that transmitted through deionised water of the same shape.

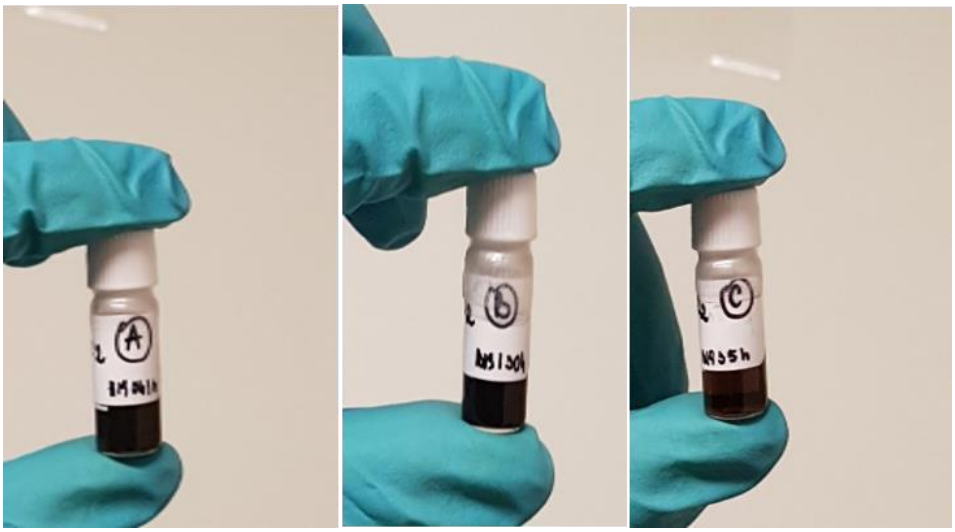

Fig. 5.5 Samples (labelled as A, B and C) of $PdSe_2$ prepared at the University of Heidelberg, Germany

Table 1: Samples properties summary

Sample	Sheet length (nm)	Number of Layers	Linear absorption coefficient (α)
A	130	15	4.83
B	54	10	4.13
C	43	7	2.04

Sample A:

The linear absorption coefficient α_0 for Sample A was 4.83 cm^{-1}.

The normalised transmission through this sample was measured using 100 nJ, 200 nJ, 300 nJ, 400 nJ and 1000nJ incident laser beam energy. The change in the normalised transmission through this sample as it moved towards and away from the focal points is shown in Figure 5.6 a-e respectively for the above intensities.

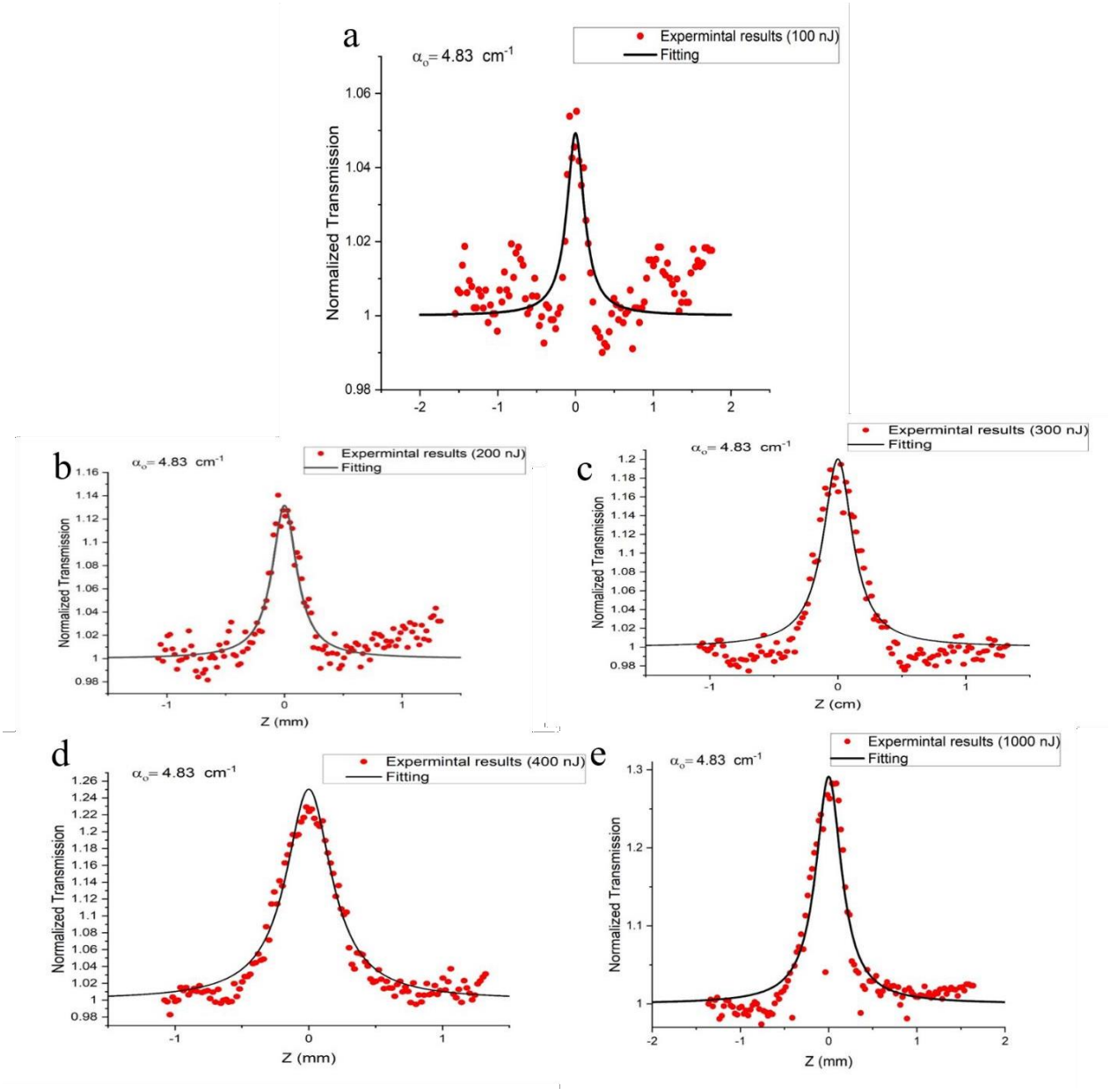

Fig. 5.6 Open-aperture Z-scans of $PdSe_2$ dispersion (Sample A). All scatter plots show experimental data, and the solid lines result from fitting.

The nonlinear absorption coefficients for Sample A for the 5 laser intensities were calculated by obtaining the best fit to the measured data

using Equation 4.4. The nonlinear absorption coefficient for each intensity is shown in Table 2.

Table 2: Nonlinear optical parameters for Sample A .

Laser wavelength	**Sample**	α_0 **cm**$^{-1}$	**Intensity nJ**	$a_{NL\ (GW/cm^{-1}}$
800nm	Sample A	4,83	100	-0.38
			200	-0.93
			300	-1.31
			400	-1.56
			1000	-1.74
Average				-1.18

Sample B:

The linear absorption coefficient α_0 for Sample "B" was 4.13 cm $^{-1}$.

The normalised transmission through this sample was measured using laser beam energies of 200 nJ, 300 nJ, 400 nJ , 500 nJ and 1000 nJ. Figure 5.7 shows the results of an open-aperture Z-scan at the above incident laser energies. A peak of transmission was observed at the focused point, indicating the saturable absorption of $PdSe_2$ at the wavelength of 800 nm.

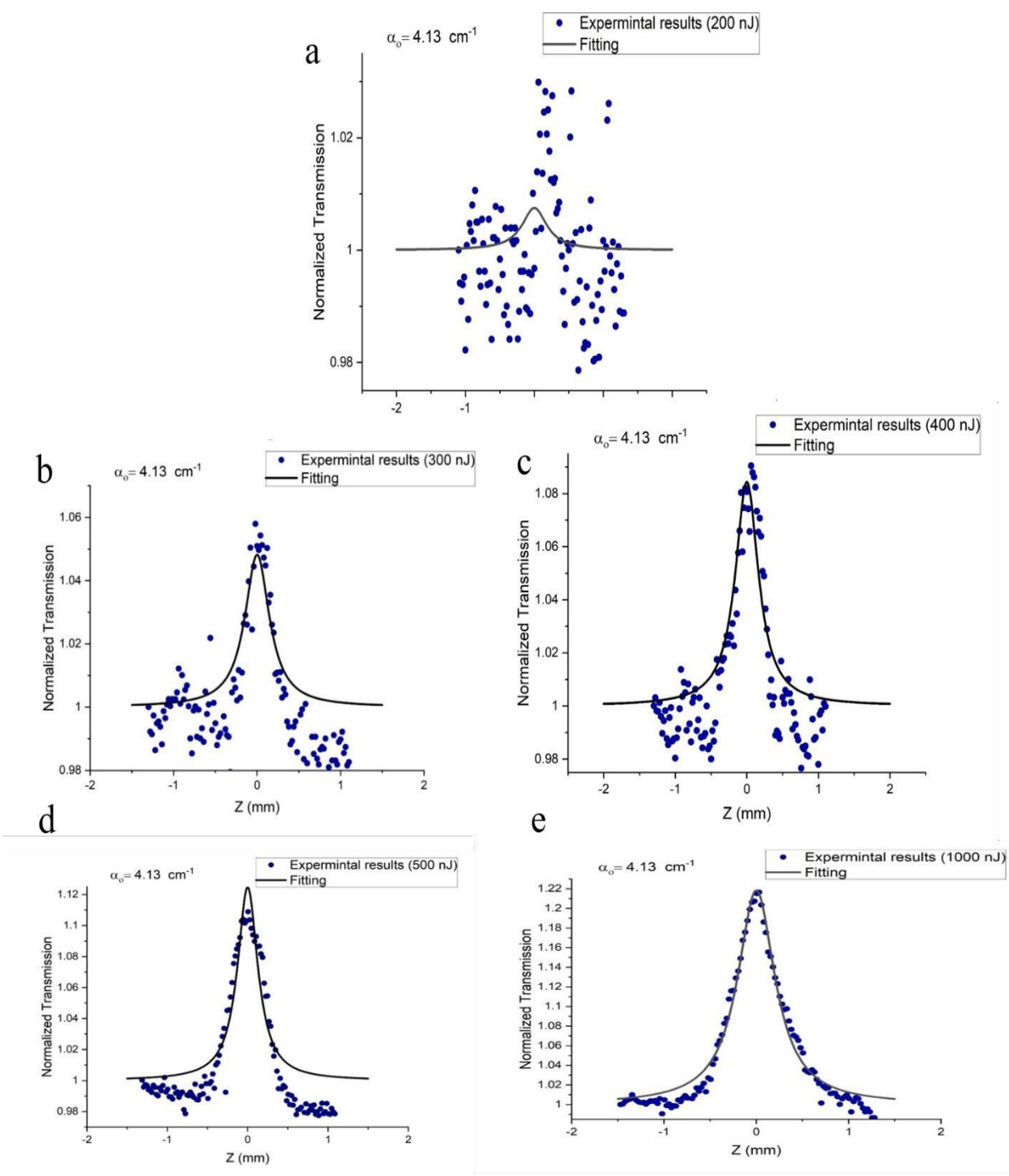

Fig. 5.7 Measurements of the Z-scan on Sample B with varying incident laser energies of 200, 300, 400, 500 and 1000 nJ.

The linear absorption coefficient was 4.13 cm^{-1}. The results were gathered with increasing laser intensity under irradiation. The 800-nm wavelength laser pulses have a duration of about 100 fs and a repetition rate of 100 kHz. They originate from a Ti: Sapphire mode-locked laser (Coherent, RegA 9000).

The non-linear absorption coefficients for the Sample B for the five laser intensities were also obtained by employing nonlinear optical propagation theory to fit the experimental data. The obtained nonlinear absorption coefficients for each intensity are shown in Table 3.

Table 3: Sample A Nonlinear Absorption Coefficients

Sample	a_0 **cm^{-1}**	**Intensity nJ**	a $_{\mathbf{NL}}$ ($\frac{\mathbf{GW}}{\mathbf{cm^{-1}}}$
Sample B	4,13	200	-0.059
		500	-0.36
		6	-0.60
		500	-0.85
		1000	-1.34
Average			-0.61

Sample C:

The linear absorption coefficient α_0 for Sample "C" was 2.046 cm^{-1}.

The normalised transmission through this sample was measured using laser beam energies of 200, 500 nJ, 600 nJ and 1000 nJ. The change in the normalised transmission through this sample as it moved towards and away from the focal points is shown in Figure 5.8 a-d respectively for the above intensities.

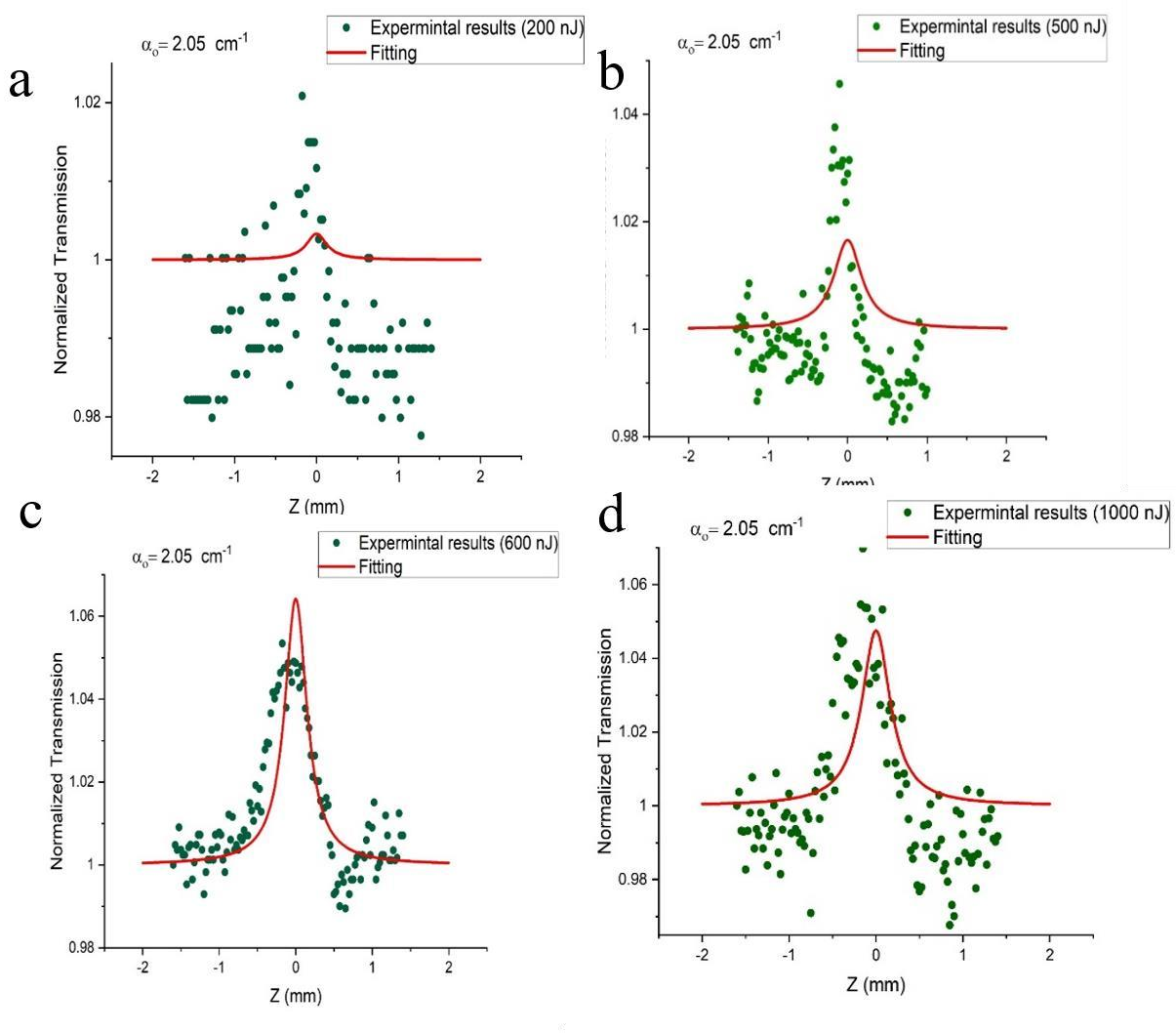

Figure 5.8 Open-aperture Z-scan curves of sample C ($PdSe_2$ dispersion) with varying incident laser energies. All scatter plots represent experimental data, whereas solid lines are from fitting.

The nonlinear absorption coefficients for Sample C for the 4 laser intensities were calculated by obtaining the best fit using nonlinear optical propagation theory. As shown in Table 4, the change in the nonlinear absorption coefficient was not consistent compared to the change in the laser beam intensity. This could be attributed to the presence of a high

level of noise in the measured data, which resulted in large residuals after the fitting process.

Table 4: The nonlinear optical parameters of Sample C.

Sample	a_0 **cm**$^{-1}$	**Intensity nJ**	a_{NL} **(GW/cm**$^{-1}$
Sample C	2.046	200	-0.021
		500	-0.11
		600	-0.39
		1000	-0.29
Average			-0.70

5.4 Pump-probe spectroscopy Results

As shown in the schematic in Figure 5.9, the pump-probe setup is based on a Reg A 9000 ultrafast laser with wavelength of 800 nm, pulseduration of 100 fs and repetition rate of 100 kHz. A beam splitter dividedthe main laser beam into two beams: a major beam to be used as a pump beam and another to be used as a probe-beam.

A motorised platform was used to delay the probe-beam by moving back and forth with Δd increment, which resulted in the time delay $\Delta t = \frac{\Delta d}{2c}$ —

where *c* is the speed of light. The pump-beam was focused on the sample for pumping and then eliminated using an aperture before the detector. The optical chopper modulated the pump-beam to enable the measurement of the probe-beam transmission in the presence and absence of the pump-beam.

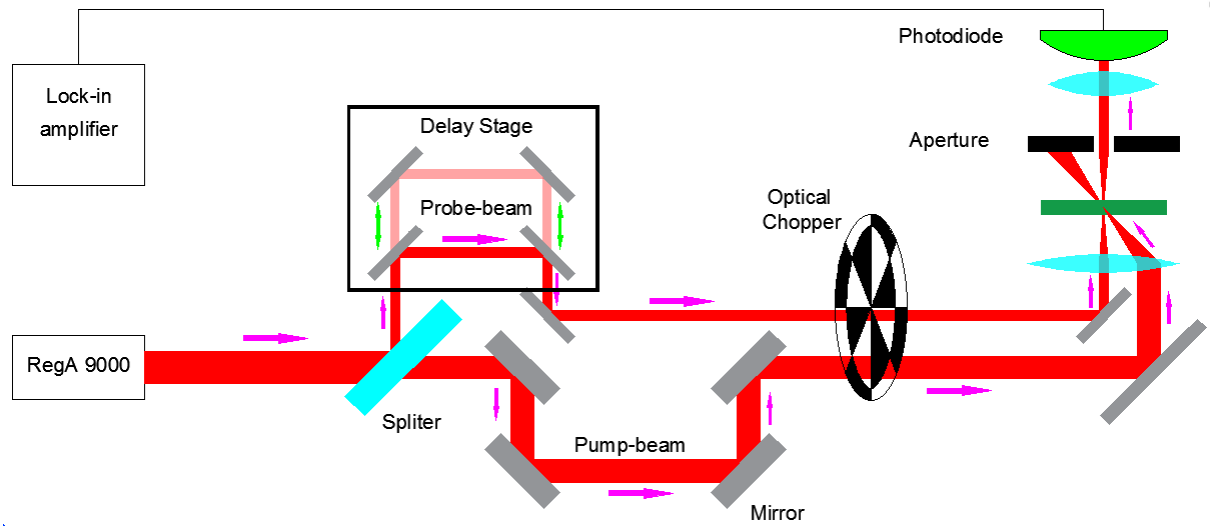

Figure 5.9 Schematic of the optical pump-probe setup that was used in this work (30)

The above pump-probe setup was used to investigate the excitation carrier dynamics of three different samples of the few-layer $PdSe_2$. Samples were

labelled as L, M and XL, with each having a different thickness, which are the B, C and A samples in the Z-scan experiments, respectively. The measurements were conducted using varying pump energies, between 140 nJ and 340 nJ. Measurements were carried out at room temperature and both the pump and probe pulses were obtained from the same laser source which had a 100-fs pulse duration.

Sample L:

The measurements for this sample were carried out with varying pump laser energies of 140 nJ, 200 nJ and 320 nJ. The energy of 320 nJ was measured twice. The carrier dynamic record for the different energy fluences is shown in Fig. 5. 10.

The few-layer $PdSe_2$ has two exponential decay components; a bi-exponential function from Equation (4.8) was used to fit the recorded data to calculate the short and long carrier life (τ_1 and τ_2 respectively). The fitting results for Sample L are shown in Table 5:

Table 5 Fitting results of pump-probe measurements on sample L.

Thickness	Set	Energy	D1 (%)	D2 (%)	t1 (ps)	t2 (ps)	Pulse duration (fs)

L	1	320 nJ	0.000	0.00	27.760	252.99	21.45
	2	140 nJ	0.000	0.00	50.616	131.428	0.40
	2	200 nJ	0.213	0.00	0.154	94.25	0.40
	2	320 nJ	18.176	0.000	0.1746	200.523	2.00
Average			4.597	0.000	19.676	169.800	6.065

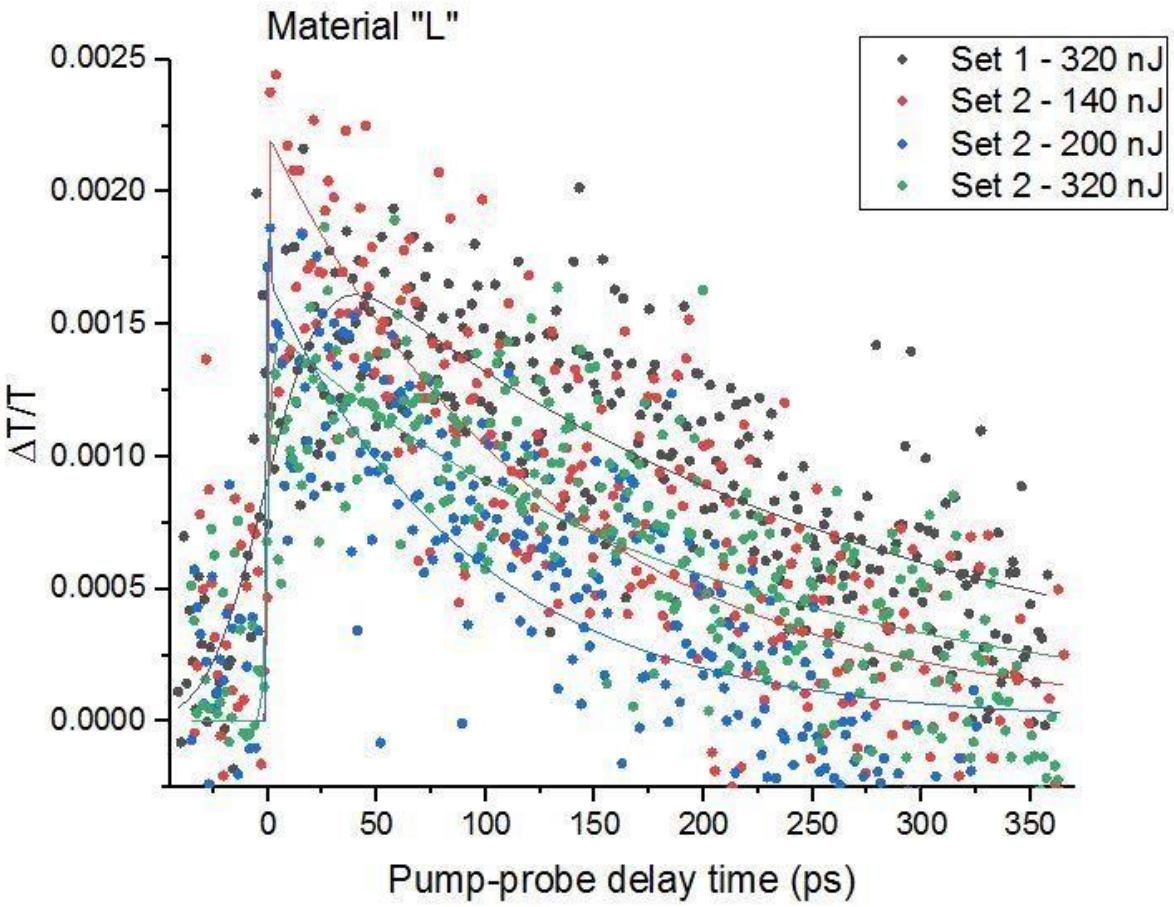

Fig. 5.10 Differential transmission of the few-layer $PdSe_2$ sample L recorded from the pump-probe experiment.

Sample M:

The measurements for this sample were carried out in one setup, where readings from 140 nJ and 200 nJ pump energy were recorded. The carrier dynamic record for the two energy fluences is shown in Figure 5. 11.

As with Sample L, assuming that the few-layer $PdSe_2$ has two exponential decay components, a bi-exponential function from Equation 4.8 was employed to fit the recorded data to calculate the short and long carrier

lives (τ_1 and τ_2 respectively). The fitting results for the Sample M are shown in Table 6:

Table 6 Fitting results of pump-probe measurements on sample M.

	Energy	D1 (%)	D2 (%)	t1 (ps)	t2 (ps)	Pulse duration (fs)
M	140 nJ	0.000	0.001	5.134	115.2795	0.400
	200 nJ	0.0000	0.001	5.562	124.032	0.400
Average		0.0001	0.001	5.348	119.657	0.400

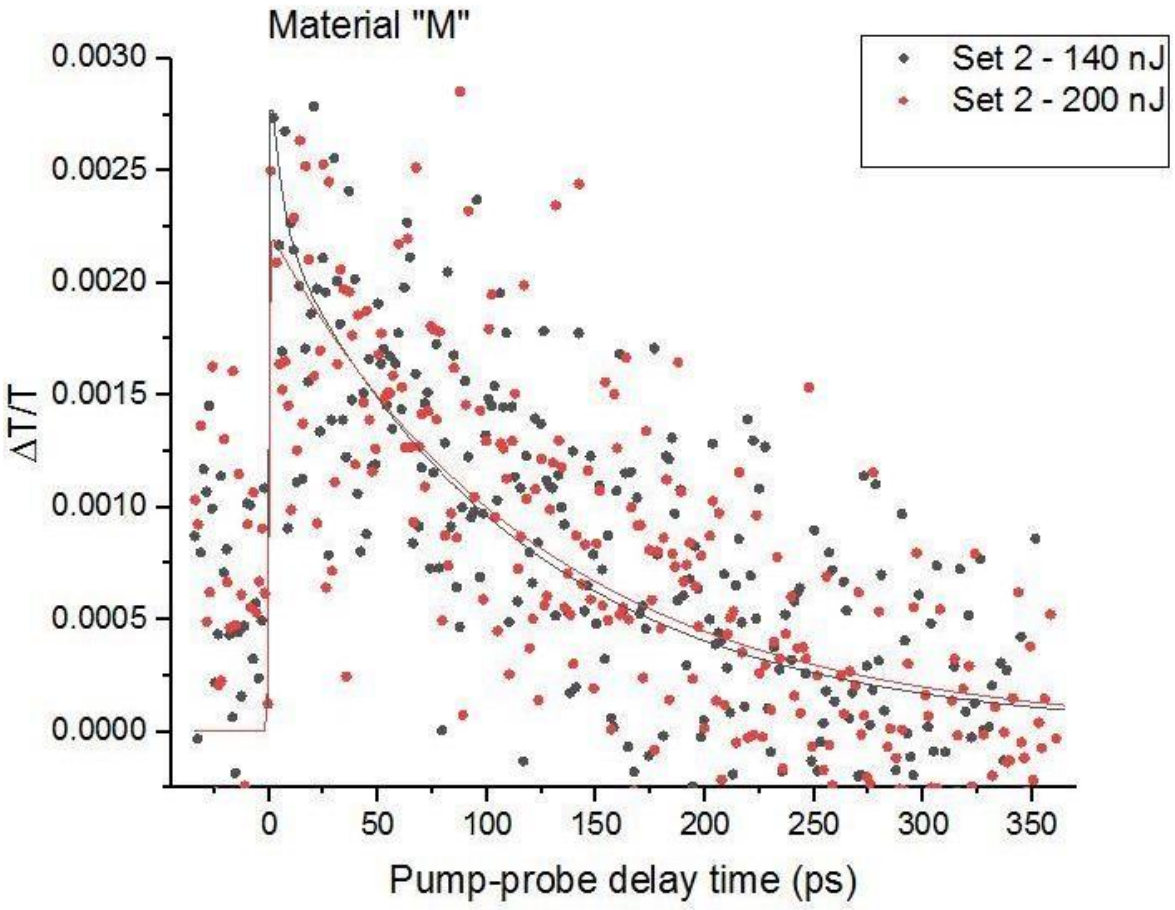

Fig. 5. 11: The differential transmission through the few-layer $PdSe_2$ sample M recorded from the pump-probe experiment.

Sample XL:

The measurements for this sample were carried out with varying pump laser energies, namely 140 nJ, 200 nJ and 320 nJ. We employed Equation 4.8 to fit the experimental data to have a view of the carrier dynamics, as shown in Figure 5. 11. To confirm the results, the same pump energy was measured for several times, labelled as ‘set 1’ ‘set 2’ and ‘set 3’.

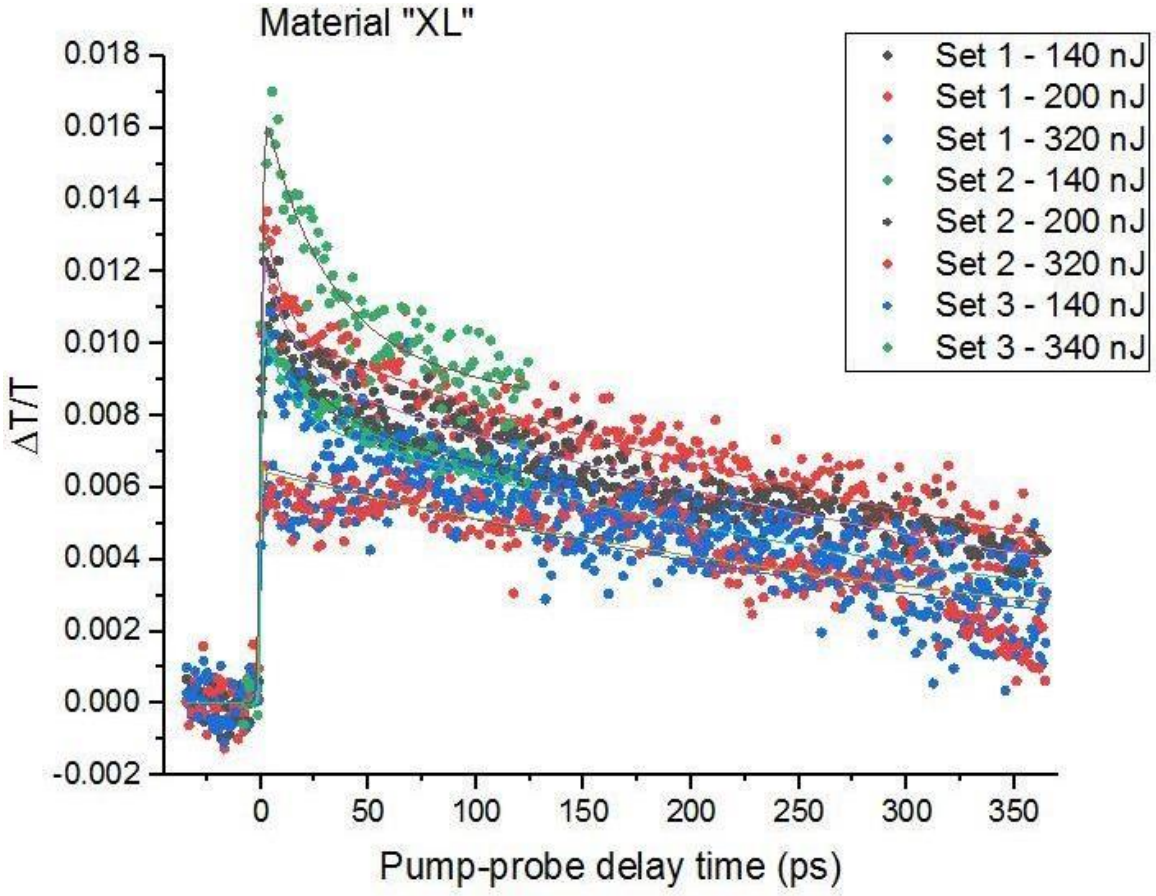

Fig. 5. 12: The differential transmission through the few-layer $PdSe_2$ sample XL recorded from the pump-probe experiment.

It is obvious that the relaxation of the excited carrier followed two steps and so a two-exponential decay model can be employed to analyses the results. The fitting curves are shown in Fig. 5.12 using solid lines. A fast and a slow relaxation time were obtained, which are summarised in Table 7. The fast relaxation times is around 10 ps, which might be attributed to the intraband relaxation of the hot carrier.

The long lifetime was fitted to be 383.50-694.68 ps, which is the recombination of the excited carrier in interband.

		Energy	D1 (%)	D2 (%)	t1 (ps)	t2 (ps)
XL	1	140 nJ	0.001	0.00	27.84	694.681
	1	200 nJ	0.001	0.005	9.25	452.950
	1	320 nJ	0.2729	0.003	0.124	389.135
	2	140 nJ	0.000	0.0042	21.131	383.50
	2	200 nJ	0.001	0.004	12.74	434.43
	2	320 nJ	3.614	0.003	0.1645	440.22
	3	140 nJ	0.001	0.004	11.14	410.055
	3	340 nJ	0.003	0.004	27.39	979.645
Average			0.48	0.0041	13.72	523.078

Conclusion

Two-dimensional (2D) nanomaterials are of particular interest in the area of nonlinear optics. Their behaviour has been shown to include a wide range of processes, such as saturable absorption and multiple-photon absorption. In this project, we used the open-aperture Z-scan, conducting experiments on the NLO response of 2D $PdSe_2$ nanosheets with various sizes and thickness to investigate their various characteristics. The measurements were based on a 100-fs laser with a repetition rate of 100 kHz at a central wavelength of 800 nm. 2D $PdSe_2$ nanosheets were obtained by using a liquid-phase exfoliation method. The studies of TEM on many samples indicate that 2D $PdSe_2$ was effectively exfoliated from its bulk.

By employing a size selection technique, 2D $PdSe_2$ nanosheets with varying size and thickness were achieved. The Z-scan measurements indicate that strong saturable absorption exits in all these 2D $PdSe_2$ nanosheets. Saturable absorption shows a dependency on the linear absorption coefficients. Additionally, an optical pump-probe technique was employed to study the carrier dynamics of these 2D $PdSe_2$ nanosheets.

Future Work

The most obvious potential continuation of this work is to continue the development of this environmentally and photochemically stable nanomaterial for use a passive mode-locker in ultrafast near-infrared fibre and free-space lasers similar to what was described and successfully demonstrated previously in the research group for graphene saturable absorber mirrors (SAMs). While commercial SESAM devices based on the nanotechnology of semiconductor epitaxial material deposition are commercially available, these have comparatively narrow windows of operation, are very expensive due to the complicated fabrication process and multi-layer structure and are increasingly photochemically unstable ass one extends operation into the near infrared. As demonstrated by the initial results obtained in this thesis, the current nanomaterial class can and will provide a viable alternative with one single active layer deposited on a metal mirror.

An initial approach would be to run computer simulations to estimate the performance of the $PdSe_2$ SAMs at different wavelengths going out to and beyond 2 μm. This could help further differentiate the current SAM from the commercial SESAMs.

Subsequent improvements to the homogeneity of spin-cast and drop-cast films are something that would greatly benefit the mode-locker device

manufacturing process.

Practical work on such an as-yet unoptimized device is ongoing in collaboration with former group-member Prof. Jun Wang, with a 1.55 μm fibre-laser being used at Shanghai Institute for Optics and Mechanics, Chinese Academy of Science.

A more thorough exploration of the nonlinear optical properties of the entire family of pentagonal 2D layered noble transition metal dichalcogenide that is air-stable would be extremely interesting. Different wavelengths, power, pulse durations and repetition rates are all potential parameters to vary. Ultrafast nonlinear spectroscopy will yield further insights into the nature and properties of fundamental excitations and their relaxation mechanisms that could reveal localised excited states similar and beyond the Trions already observed in some 2D transition-metal dichalcogenide semiconductors .

References

(1) Personal protective equipment for engineered nanoparticles (https://safety.fsu.edu/safety_manual/supporting_docs/PPE%20for%20nanoparticles%20-%20AIHA.pdf)

(2) Zhang, H., Ma, P., Zhu, M., Zhang, W., Wang, G., & Fu, S. (2020). Palladium selenide as a broadband saturable absorber for ultra-fast photonics. *Nanophotonics*, *9*(8), 2557-2567. https://doi.org/10.1515/nanoph-2020-0116

(3) Mao, H. Y., Laurent, S., Chen, W., Akhavan, O., Imani, M., Ashkarran, A. A., & Mahmoudi, M. (2013). Graphene: promises, facts, opportunities, and challenges in nanomedicine. *Chemical reviews*, *113*(5), 3407-3424.113. 10.1021/cr300335p.

(4) Linnan, Jia & Wu, Jiayang & Tieshan, Yang & Jia, Baohua & Moss, David. (2020). Ultra-large Kerr optical nonlinearity in 2D PdSe 2 films.

(5) Oyedele, A. D., Yang, S., Liang, L., Puretzky, A. A., Wang, K., Zhang, J., ... & Xiao, K. (2017). PdSe2: pentagonal two-dimensional layers with high air stability for electronics. *Journal of the American Chemical Society*, *139*(40), 14090-14097.

(6) Locatelli, Andrea & Knox, Kevin & Cvetko, Dean & Menteş, Tevfik & Niño, Miguel & Wang, Shancai & Yilmaz, Mehmet & Kim, Philip & Osgood, Richard & Morgante, Alberto. (2010). Corrugation in Exfoliated Graphene: An Electron Microscopy and Diffraction Study. ACS nano. 4. 4879-89. 10.1021/nn101116

(7) Zhang, G.; Amani, M.; Chaturvedi, A.; Tan, C.; Bullock, J.; Song, X.; Kim, H.; Lien, D.-H.; Scott, M. C.; Zhang, H.; Javey, A. Optical and electrical properties of two-dimensional palladium diselenide. Appl. Phys. Lett. 2019, 114, 253102.

(8) Locatelli, A., Knox, K. R., Cvetko, D., Mentes, T. O., Nino, M. A., Wang, S., ... & Morgante, A. (2010). Corrugation in exfoliated graphene: an electron microscopy and diffraction study. *ACS nano*, *4*(8), 4879-4889.

(9) Jia, L., Wu, J., Yang, T., Jia, B., & Moss, D. J. (2020). Large third-order optical kerr nonlinearity in nanometer-thick PdSe2 2D dichalcogenide films: implications for nonlinear photonic devices. *ACS Applied Nano Materials*, *3*(7), 6876-6883.

(10) Jia, L., Wu, J., & Moss, D. J. (2021). Ultra-large Optical Kerr Nonlinearity in 2D PdSe2 Dichalcogenide Thin Films for Integrated Nonlinear Photonics (doi: 10.20944/preprints202103.0021.v1).

(11) Geim, A. K., & Novoselov, K. S. (2010). The rise of graphene. In *Nanoscience and technology: a collection of reviews from nature journals* (pp. 11-19). Available at http://www.nature.com/articles/nmat1849 1, 5, 6, 7, 8

(12) Soldano, C., Mahmood, A., & Dujardin, E. (2010). Production, properties and potential of graphene. *Carbon*, *48*(8), 2127-2150. Available: https://linkinghub.elsevier.com/retrieve/pii/S0008622310000928 6

(13) Abergel, D. S. L., Apalkov, V., Berashevich, J., Ziegler, K., & Chakraborty, T. (2010). Properties of graphene: a theoretical perspective. *Advances in Physics*, *59*(4), 261-482. Available: https://www.tandfonline.com/doi/full/10.1080/00018732.2010.487978 6

(14) Neto, A. C., Guinea, F., Peres, N. M., Novoselov, K. S., & Geim, A. K. (2009). The electronic properties of graphene. *Reviews of modern physics*, *81*(1), 109. Available: https://link.aps.org/doi/10.1103/RevModPhys.81.109 6, 8

(15) Sprinkle, M., Siegel, D., Hu, Y., Hicks, J., Tejeda, A., Taleb-Ibrahimi, A., ... & Conrad, E. H. (2009). First direct observation of a nearly ideal graphene band

structure. *Physical Review Letters*, *103*(22), 226803.. Available: https://link.aps.org/doi/10.1103/PhysRevLett.103.226803 6

(16) Bolotin, K. I., Sikes, K. J., Jiang, Z., Klima, M., Fudenberg, G., Hone, J., ... & Stormer, H. L. (2008). Ultrahigh electron mobility in suspended graphene. *Solid state communications*, *146*(9-10), 351-355. Available: https: //linkinghub.elsevier.com/retrieve/pii/S0038109808001178 7

(17) Zhang, Huanian, Ma, Pengfei, Zhu, Mingxiao, Zhang, Wenfei, Wang, Guomei and Fu, Shenggui. "Palladium selenide as a broadband saturable absorber for ultra-fast photonics" Nanophotonics, vol. 9, no. 8, 2020, pp. 2557-2567. https://doi.org/10.1515/nanoph-2020-0116

(18) Zhang, H., Ma, P., Zhu, M., Zhang, W., Wang, G., & Fu, S. (2020). Palladium selenide as a broadband saturable absorber for ultra-fast photonics. *Nanophotonics*, *9*(8), 2557-2567. https://doi.org/10.1515/nanoph-2020-0267

(19) Linnan, Jia & Wu, Jiayang & Tieshan, Yang & Jia, Baohua & Moss, David. (2020). Ultra-large Kerr optical nonlinearity in 2D PdSe 2 films.

(20) Jia, L., Wu, J., & Moss, D. J. (2021). Ultra-large Optical Kerr Nonlinearity in 2D PdSe2 Dichalcogenide Thin Films for Integrated Nonlinear Photonics (doi: 10.20944/preprints202103.0021.v1).

(21) Oyedele, A. D., Yang, S., Liang, L., Puretzky, A. A., Wang, K., Zhang, J., ... & Xiao, K. (2017). PdSe2: pentagonal two-dimensional layers with high air stability for electronics. *Journal of the American Chemical Society*, *139*(40), 14090-14097.

(22) Zhang, G., Amani, M., Chaturvedi, A., Tan, C., Bullock, J., Song, X., ... & Javey, A. (2019). Optical and electrical properties of two-dimensional palladium diselenide. *Applied Physics Letters*, *114*(25), 253102.

(23) Jiang, S., Xie, C., Gu, Y., Zhang, Q., Wu, X., Sun, Y., ... & Zhang, Y. (2019). Anisotropic growth and scanning tunneling microscopy identification of ultrathin even-layered PdSe2 ribbons. *Small*, *15*(45), 1902789.

(24) Smith, Ronan, Liquid Phase Exfoliation and Dispersion of Two -Dimensional Material, Trinity Collage Dublin, School of Physics, 2014

(25) Sheik-Bahae, M., Said, A. A., & Van Stryland, E. W. (1989). High-sensitivity, single-beam n 2 measurements. *Optics letters*, *14*(17), 955-957 (https://www.osapublishing.org/ol/abstract.cfm?uri=ol-14-17-955)

(26) Wang, G., Baker-Murray, A. A., & Blau, W. J. (2019). Saturable absorption in 2D nanomaterials and related photonic devices. *Laser & Photonics Reviews*, *13*(7), 1800282 (https://doi.org/10.1002/lpor.201800282)

(27) Wang, J., Sheik-Bahae, M., Said, A. A., Hagan, D. J., & Van Stryland, E. W. (1994). Time-resolved Z-scan measurements of optical nonlinearities. *JOSA B*, *11*(6), 1009-1017.

(28) Wang, G., Wang, K., Szydłowska, B. M., Baker-Murray, A. A., Wang, J. J., Feng, Y., ... & Blau, W. J. (2017). Ultrafast nonlinear optical properties of a graphene saturable mirror in the 2 μm wavelength region. *Laser & Photonics Reviews*, *11*(5), 1700166 (11. 10.1002/lpor.201770051)

(29) Neethling, P. H. (2005). Determining non-linear optical properties using the Z-scan technique (Doctoral dissertation, Stellenbosch: University of Stellenbosch).

(30) WANG, GAOZHONG, Third-order Nonlinear Optical Response and Ultrafast Carrier Dynanics of 2D Materials, Trinity College Dublin. School of Physics. PHYSICS, 2018

(31) Lytle, F. E., Parrish, R. M., & Barnes, W. T. (1985). An introduction to time-resolved pump/probe spectroscopy. *Applied spectroscopy*, *39*(3), 444-451.

(32) Li, T. (2014). *Ultrafast laser spectroscopy in complex solid state materials* (Doctoral dissertation, Iowa State University). Web. doi:10.2172/1226570.

(33) Wang, G., Wang, K., Szydłowska, B. M., Baker-Murray, A. A., Wang, J. J., Feng, Y., ... & Blau, W. J. (2017). Ultrafast nonlinear optical properties of a graphene saturable mirror in the 2 μm wavelength region. *Laser & Photonics Reviews*, *11*(5), 1700166.

(34) Wang, G., Liang, G., Baker-Murray, A. A., Wang, K., Wang, J. J., Zhang, X., ... & Blau, W. J. (2018). Nonlinear optical performance of few-layer molybdenum diselenide as a slow-saturable absorber. *Photonics Research*, *6*(7), 674-680.

(35) Wang, K., Wang, J., Fan, J., Lotya, M., O'Neill, A., Fox, D., ... & Blau, W. J. (2013). Ultrafast saturable absorption of two-dimensional MoS2 nanosheets. *ACS nano*, *7*(10), 9260-9267.

(36) Wang, K., Szydłowska, B. M., Wang, G., Zhang, X., Wang, J. J., Magan, J. J., ... & Blau, W. J. (2016). Ultrafast nonlinear excitation dynamics of black phosphorus nanosheets from visible to mid-infrared. *ACS nano*, *10*(7), 6923-6932.

(37) Szydłowska, B. M., Tywoniuk, B., & Blau, W. J. (2018). Size-dependent nonlinear optical response of black phosphorus liquid phase exfoliated nanosheets in nanosecond regime. *ACS Photonics*, *5*(9), 3608-3612.

(38) Radu, M. Schleeger, C. Bolwien and J. Heberle, Photochem. Photobiol. Sci., 2009, 8, 1517

(39) Wang, K., Szydłowska, B. M., Wang, G., Zhang, X., Wang, J. J., Magan, J. J., ... & Blau, W. J. (2016). Ultrafast nonlinear excitation dynamics of black phosphorus nanosheets from visible to mid-infrared. *ACS nano*, *10*(7), 6923-6932.